

REPORT DOCUMENTATION PAGE				Form Approved OMB No. 0704-0188	
Public reporting burden for this collection of information is estimated to average 1 hour per response, including the time for reviewing instructions, searching existing data sources, gathering and maintaining the data needed, and completing and reviewing this collection of information. Send comments regarding this burden estimate or any other aspect of this collection of information, including suggestions for reducing this burden to Department of Defense, Washington Headquarters Services, Directorate for Information Operations and Reports (0704-0188), 1215 Jefferson Davis Highway, Suite 1204, Arlington, VA 22202-4302. Respondents should be aware that notwithstanding any other provision of law, no person shall be subject to any penalty for failing to comply with a collection of information if it does not display a currently valid OMB control number. PLEASE DO NOT RETURN YOUR FORM TO THE ABOVE ADDRESS.					
1. REPORT DATE (DD-MM-YYYY) 29-03-2007		2. REPORT TYPE Technical Paper and Briefing Charts		3. DATES COVERED (From - To)	
4. TITLE AND SUBTITLE  Advancements in Theoretical Models of Confined Vortex Flowfields				5a. CONTRACT NUMBER FA8650-05-C-2612	
				5b. GRANT NUMBER	
				5c. PROGRAM ELEMENT NUMBER	
6. AUTHOR(S) Joshua W. Batterson, Brian A. Maicke and Joseph Majdalani (Univ. of Tenn. Space Inst.)				5d. PROJECT NUMBER 503305AP	
				5e. TASK NUMBER	
				5f. WORK UNIT NUMBER	
7. PERFORMING ORGANIZATION NAME(S) AND ADDRESS(ES)  Orbital Technologies Corp (ORBITEC) Space Center 1212 Fourier Drive Madison WI 53717				8. PERFORMING ORGANIZATION REPORT NUMBER  AFRL-PR-ED-TP-2007-222	
9. SPONSORING / MONITORING AGENCY NAME(S) AND ADDRESS(ES)  Air Force Research Laboratory (AFMC) AFRL/PRS 5 Pollux Drive Edwards AFB CA 93524-70448				10. SPONSOR/MONITOR'S ACRONYM(S)	
				11. SPONSOR/MONITOR'S NUMBER(S) AFRL-PR-ED-TP-2007-222	
12. DISTRIBUTION / AVAILABILITY STATEMENT  Distribution A: Approved for Public Release; distribution unlimited (Public Affairs No. 07146A).					
13. SUPPLEMENTARY NOTES Presented at the JANNAF 54 <sup>th</sup> Propulsion Meeting/3 <sup>rd</sup> Liquid Propulsion Subcommittee/2 <sup>nd</sup> Spacecraft Propulsion Subcommittee/5 <sup>th</sup> Modeling and Simulation Subcommittee Joint Meeting, Denver, CO, 14-17 May 2007.					
14. ABSTRACT In this article, we review some of the theoretical solutions used to describe swirl dominated flows in both unidirectional and bidirectional flow orientations. This short survey starts with the Rankine vortex and culminates in the presentation of a compressible solution of the bidirectional vortex. After classifying representative swirl motions as external or internal depending on physical boundary conditions, their commonalities are identified along with their relevance to either geophysical or industrial applications. For example, all swirl dominated flows comprise a forced vortex core centered around their axis of rotation. The core is due to viscous forces and increases in size with successive increases in viscosity. It is delineated by the point where the swirl velocity reaches its maximum. Within the forced vortex core, the tangential velocity is linearly proportional to the radius, a characteristic of rigid body rotation. Outside the forced vortex core, the tangential velocity gradually becomes inversely proportional to the radius, thus exhibiting a free vortex tail. In internal flows, this free, irrotational tail is clipped at the boundaries in fulfillment of the no slip requirement. In external flows, it extends out to infinity. Finally, all swirl dominated flows decay axially and their vorticity is confined to either the core vortex or wall boundary layers. These will be described in the context of the bidirectional vortex confined in a cylindrical chamber. What is most prevalent here, and perhaps, what sets the analysis of the bidirectional vortex apart lies in its true prediction of essential flow attributes directly from first principles. Unlike other studies that require conjecture or post-diction, for example, in estimating or adjusting the maximum swirl velocity and thickness of the core vortex to fit a given flow pattern (e.g., the Rankine vortex), these are obtained directly from the asymptotic solution of the tangential boundary layer equation for the bidirectional vortex. We also identify the key similarity parameters that control the problem, including the inflow parameter, $\kappa$ , and the vortex Reynolds number, $V$ . The latter combines the mean flow Reynolds number and the product of the swirl number and chamber aspect ratio. In this study, the core and sidewall boundary layers are quantified as function of $V$ . The compressible solution is also obtained assuming a Rayleigh-Janzen expansion in the inflow Mach number squared.					
15. SUBJECT TERMS					
16. SECURITY CLASSIFICATION OF:			17. LIMITATION OF ABSTRACT  SAR	18. NUMBER OF PAGES  67	19a. NAME OF RESPONSIBLE PERSON Dr. Richard Cohn
a. REPORT Unclassified	b. ABSTRACT Unclassified	c. THIS PAGE Unclassified			19b. TELEPHONE NUMBER (include area code) N/A

# Advancements in Theoretical Models of Confined Vortex Flowfields

Joshua W. Batterson,<sup>\*</sup> Brian A. Maicke<sup>†</sup> and Joseph Majdalani<sup>‡</sup>  
*University of Tennessee Space Institute, Tullahoma, TN 37388*

In this article, we review some of the theoretical solutions used to describe swirl dominated flows in both unidirectional and bidirectional flow orientations. This short survey starts with the Rankine vortex and culminates in the presentation of a compressible solution of the bidirectional vortex. After classifying representative swirl motions as external or internal depending on physical boundary conditions, their commonalities are identified along with their relevance to either geophysical or industrial applications. For example, all swirl dominated flows comprise a forced vortex core centered around their axis of rotation. The core is due to viscous forces and increases in size with successive increases in viscosity. It is delineated by the point where the swirl velocity reaches its maximum. Within the forced vortex core, the tangential velocity is linearly proportional to the radius, a characteristic of rigid body rotation. Outside the forced vortex core, the tangential velocity gradually becomes inversely proportional to the radius, thus exhibiting a free vortex tail. In internal flows, this free, irrotational tail is clipped at the boundaries in fulfillment of the no slip requirement. In external flows, it extends out to infinity. Finally, all swirl dominated flows decay axially and their vorticity is confined to either the core vortex or wall boundary layers. These will be described in the context of the bidirectional vortex confined in a cylindrical chamber. What is most prevalent here, and perhaps, what sets the analysis of the bidirectional vortex apart lies in its true prediction of essential flow attributes directly from first principles. Unlike other studies that require conjecture or post-diction, for example, in estimating or adjusting the maximum swirl velocity and thickness of the core vortex to fit a given flow pattern (e.g., the Rankine vortex), these are obtained directly from the asymptotic solution of the tangential boundary layer equation for the bidirectional vortex. We also identify the key similarity parameters that control the problem, including the inflow parameter,  $\kappa$ , and the vortex Reynolds number,  $V$ . The latter combines the mean flow Reynolds number and the product of the swirl number and chamber aspect ratio. In this study, the core and sidewall boundary layers are quantified as function of  $V$ . The compressible solution is also obtained assuming a Rayleigh-Janzen expansion in the inflow Mach number squared.

## Nomenclature

$a$	= chamber radius
$A_i$	= inlet area
$b$	= chamber outlet radius
$l$	= chamber aspect ratio, $L/a$
$\bar{p}$	= normalized pressure, $\bar{p}/(\rho U^2)$
$\bar{Q}_i$	= inlet volumetric flow rate
$\bar{Q}_i$	= normalized volumetric flow rate, $\bar{Q}_i/(Ua^2) = \sigma^{-1}$
$Re$	= injection Reynolds number, $Ua/\nu = 1/\varepsilon$

<sup>\*</sup>Graduate Research Assistant.

<sup>†</sup>Graduate Research Assistant.

<sup>‡</sup>Jack D. Whitfield Professor of High Speed Flows, Department of Mechanical, Aerospace and Biomedical Engineering. Fellow ASME.

$r, z$	= normalized radial or axial coordinates, $\bar{r}/a, \bar{z}/a$
$S$	= swirl number, $\pi ab / A_i = \pi\beta\sigma$
$\mathbf{u}$	= normalized velocity $(\bar{u}_r, \bar{u}_z, \bar{u}_\theta)/U$
$u_\theta$	= normalized swirl/spin/tangential velocity, $\bar{u}_\theta/U$
$U$	= mean inflow velocity, $\bar{u}_\theta(a, L)$
$V$	= vortex Reynolds number, $Q_i Re(a/L) = (\varepsilon\sigma l)^{-1}$

#### Greek

$\beta$	= normalized outlet radius, $b/a$
$\delta$	= $\eta$ – rescaled radius of the viscous core
$\delta_c$	= normalized core radius, $\bar{\delta}_c/a$
$\delta_w$	= wall tangential boundary layer thickness, $\bar{\delta}_w/a$
$\varepsilon$	= perturbation parameter, $1/Re = \nu/(Ua)$
$\kappa$	= inflow parameter, $Q_i/(2\pi l) = (2\pi\sigma l)^{-1}$
$\lambda$	= $\eta$ – rescaled wall layer thickness, $\bar{\lambda}/a$
$\nu$	= kinematic viscosity, $\mu/\rho$
$\eta$	= transformed variable, $\pi r^2$
$\rho$	= density
$\sigma$	= modified swirl number, $Q_i^{-1} = S/(\pi\beta)$

#### Subscripts

$i$	= inlet property
$r$	= radial component or partial derivative
$z$	= axial component or partial derivative
$\theta$	= azimuthal component or partial derivative
$\bar{\phantom{x}}$	= overbars denote dimensional variables

#### Superscripts

$c$	= composite
$i$	= inner core
$w$	= near sidewall

## I. Introduction

THE flow patterns associated with swirl dominated vortex motions have long been of interest to scientists and engineers who have constantly strived to duplicate naturally occurring phenomena and import their performance enhancing effects to thermal and mass transport applications. In reality, swirl patterns vary over widely dissimilar length and time scales depending on the physical context, be it *geophysical* or *industrial*, *external* or *internal*. In meteorology, for example, one is interested in better understanding the formation of tornadoes, waterspouts, dust devils, fire whirls, typhoons, hurricanes, or tropical cyclones (see Penner [1]). In astrophysics, one is interested in the helical trajectories of celestial bodies, cosmic jets, galactic pinwheels, and the ever expanding and accelerating corkscrew motion of the universe (see Königl [2] and Kirshner [3]). In industrial applications, one attempts to trigger swirl using a variety of devices and concepts for the purpose of improving mixing, heating or cooling, combustion or separation efficiencies, and chemical filtration or dispensing. Devices used for triggering and sustaining helical vortices are constantly developed and optimized. These include swirler blades, curved vanes, vortex generators, twisted tape inserts, triangular winglets, propellers, coiled wires, tangential injectors, and other vortex trippers, to name a few. The resulting swirling motions can be further characterized as *unidirectional* or *bidirectional*, as in the case of cyclonic motion (Reydon and Gauvin [4]). The latter underlies centrifugal separation processes, cyclonic furnaces, and the self-cooling thrust engine developed by Chiaverini et al. [5-7]. While multidirectional vortex motions can also be triggered [8], their use is strictly limited due to the difficulties associated with their flow stability and control.

In studying unidirectional columnar vortices, one is interested in predicting their inception, evolution, stability and breakdown (Harvey [9]). The two predominant modes of breakdown are the S- and B-types, named after the *spiral* and *bubble* shaped patterns that accompany the disruption of columnar vortex filaments. These two disruption

modes can be sequentially triggered with successive increases in the Reynolds and swirl numbers. The standard swirl number  $S$  is a dimensionless parameter that scales with the ratio of tangential and axial momentum forces. In addition to the S- and B-type instabilities, other breakdown patterns, such as the double helix, have been reported by Sarpkaya [10] and others, including Leibovich [11,12]. What is important to note here is that vortex breakdown is often accompanied by flow expansion and swelling that can be effectively modulated to control flames and, therefore, improve the combustion efficiency of swirling jets.

As described by Lilley [13], swirling jets can be markedly beneficial to the operation of industrial furnaces, utility boilers, gas turbines, and other swirl combustors. Here too, a distinction can be made between the fuel and oxidizer modes of injection, specifically, between *coswirling* and *counterswirling* jet configurations. The latter leads to reduced speed at the fuel-oxidizer interjet layer. The coswirling arrangement is often favored due to its ability to promote higher combustion efficiency and reduce sensitivity to changes in operating conditions (Gupta, Lilley and Syred [14]; Durbin and Ballal [15]).

Interestingly, it is a coswirling, fully reversing, bidirectional flow configuration that lies beneath the operation of gaseous and hydro cyclones (Fig. 1); these are ubiquitously used in the petrochemical, mineral, and powder processing industries (e.g., in product recovery, scrubbing, and dedusting). It is also a coswirling arrangement that characterizes the concentric pair of coaxial vortices established in the Vortex Combustion Cold-Wall Chamber (VCCWC) developed by Chiaverini et al. [5-7] (Fig. 2). This pair consists of an outer, headwall-directed, annular vortex and an inner, nozzle-directed, tubular vortex that are separated by a rotating, axially non-translating fluid interface known as the *mantle*. A similar spinning wheel separates the updraft from the downdraft in cyclonic tubes and furnaces, with the two most prevalent configurations being *conical* and *cylindrical* (Fig. 1).

While flow separation cyclones dispose of two outlets, the *vortex finder* and the *spigot* (where the heavier mixture particles are collected), the bidirectional vortex induced in the VCCWC enables the flow to exit through one section only, the *nozzle*. Another distinguishing feature of the VCCWC is the flow being reactive, the *outer, annular vortex* consisting of an oxidizer fluid, and the *inner, tubular vortex* consisting of a combustible mixture and products; these hot gases remain separated from the outer, cool vortex by virtue of the mantle, the interface between the chamber's outer and inner coswirling streams.

The outer and inner vortices established in the bidirectional swirl chamber must not be construed for or confused with the *outer, free vortex* and *inner, forced vortex* motions that characterize all swirl dominated flows, unidirectional or bidirectional. In fact, one of the common features that are shared by all swirl induced flows is the presence of a forced vortex core surrounding their axis of rotation (see Lewellen [16] or Vatistas et al. [17-19]). The thickness of the core  $\delta_c$  is commensurate with viscous intensity and diminishes with successive increases in the Reynolds number  $Re = Ua/\nu$ . Conversely, the maximum swirl velocity which, by definition, occurs at the outer

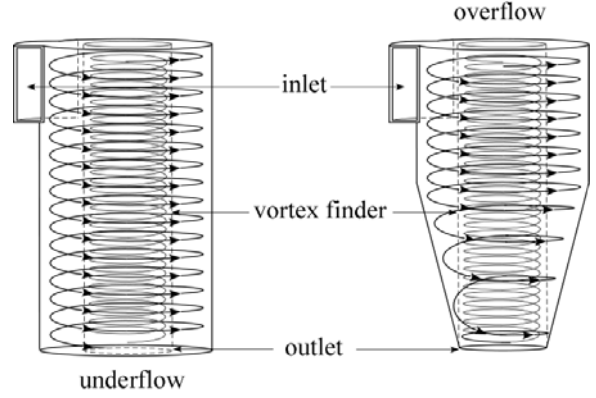


Figure 1. Cylindrical and conical cyclone separators.

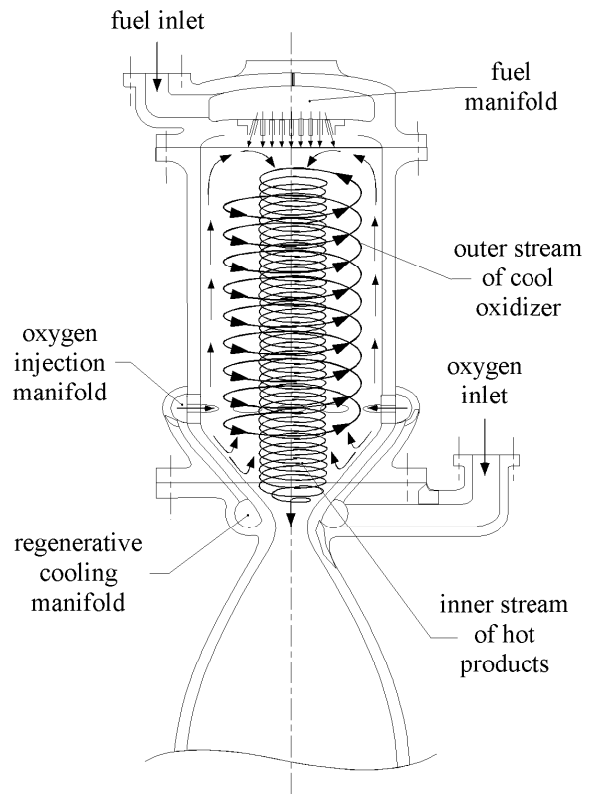


Figure 2. Sketch of ORBITEC's Vortex Combustion Cold-Wall Chamber (VCCWC) by Chiaverini et al. [5-7].

edge of the forced vortex core, increases with the Reynolds number. So while the relationship between the tangential velocity  $\bar{u}_\theta$  and radial distance from the axis of rotation  $\bar{r}$  is nearly linear within the forced vortex core, it becomes inversely proportional in the outer, free vortex region (see Fig. 3). The ensuing free vortex tail continues to diminish asymptotically in unbounded flows but is rapidly clipped in the presence of solid boundaries (Fig. 3a). Due to the continually increased shearing ascribed to the forced vortex mechanism as  $\bar{r} \rightarrow 0$ ,  $\bar{u}_\theta$  is also trimmed at the centerline.

Other distinguishing features of swirl dominated flows are their axial decay and their vorticity being mostly confined to either their core or wall boundary layers. Almost paradoxically, the outer region that is adequately represented by a free vortex is nearly irrotational. In the case of the bidirectional vortex, any vorticity in the outer region cannot originate from the spinning motion, but rather, from the order of magnitude weaker axial and radial velocity fields.

A technological vantage point of the VCCWC flowfield is that, by virtue of the inner swirl peaking in the core region, fuel residence time is prolonged, mixing is enhanced, and improved performance and thrust generation are promoted. Meanwhile, the outer annular vortex provides a thermal barrier that mitigates heating of the walls, thus alleviating thermal cycling and promoting longer life, durability and reduced weight. The increased angular shearing rates near the core are thusly put to good use in this propulsive application (Flinn [20] and Chiaverini et al. [5]).

Despite the large number of numerical and experimental investigations of swirl dominated flows, a much smaller subset has been devoted to the advancement of suitable mathematical models to describe these motions analytically. The present article constitutes one such example. The reason could be attributed to the complexity of equations that arise in the presence of a third flowfield element, namely, that of swirl. Most familiar closed-form solutions are either planar or axisymmetric. In this article, we intend to review some of these solutions, at least the ones most relevant to swirl dominated motions, starting with unidirectional flows, and then explore those applicable to bidirectional vortices. Particular emphasis will be placed on the development of core and sidewall boundary layer approximations, and the inevitable treatment of compressible flow behavior.

## II. Classical Unidirectional Solutions

Some of the classical solutions for describing unidirectional vortex motions are known as the Rankine, Oseen-Lamb, and Burgers-Rott vortices.

### A. Rankine Combined Vortex (1858)

One of the earliest theoretical studies of swirl dynamics dates back to 1858 and the work of Rankine [21]. Accordingly, an external, unidirectional swirling motion can be broken into two parts: a free and a forced vortex region. On the one hand, the forced vortex core exhibits solid body rotation and linearly increases with the radius up to a maximum value at  $\bar{r} = \delta_c$ . On the other hand, the free vortex characterizes the outer, far field region where the swirl velocity diminishes inversely with the radius. The combination of these two separate flow regimes leads to a piecewise representation of the velocity profile. Often referred to as the Rankine combined vortex, this solution can be written as

$$\frac{\bar{u}_\theta(\bar{r})}{\bar{u}_c} = \begin{cases} \frac{\bar{r}}{\delta_c} & (\bar{r} \leq \delta_c) \\ \frac{\delta_c}{\bar{r}} & (\bar{r} > \delta_c) \end{cases} \quad (1)$$

where  $\bar{u}_c \equiv (\bar{u}_\theta)_{\max}$  is the maximum tangential velocity, and  $\delta_c$  is the radius of the forced vortex extending to the point where the peak velocity is reached (see Fig. 4). Pursuant to this model, both the magnitude and position of the maximum swirl velocity must be known beforehand. This information can be extracted from experimental or

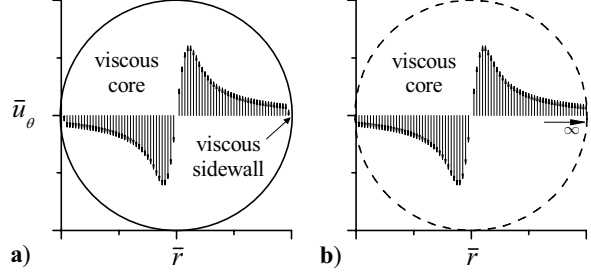


**Figure 3. Qualitative behavior of the unidirectional or bidirectional swirl velocities in a) internal, confined and b) external, unbounded flows. No dimensions are shown deliberately.**

numerical data and then used to adjust the flow pattern as desired. Despite its simplicity and reliance on post-diction, the Rankine approximation is still being used as an initial or baseline model and, despite its neglect of radial and axial motions, continues to serve as a rudimentary approximation for tornadoes and hurricanes [22]. Because the tail of the Rankine vortex is irrotational, all of the vorticity is confined to the core region. Furthermore, due to the linear dependence of  $\bar{u}_\theta$  on  $\bar{r}$ , the vorticity remains constant for  $\bar{r} \leq \delta_c$ . Finally, the essential patching of the profiles at the edge of the forced vortex region leads to discontinuities in several flowfield variables. In order to present a more compact representation of the Rankine vortex, one may use the forced vortex core radius as the only available length scale to normalize  $\bar{r}$ , and the maximum tangential speed to rescale the velocity. At the outset, one may put

$$u_\theta = \begin{cases} r & (r \leq 1) \\ \frac{1}{r} & (r > 1) \end{cases} \quad r = \frac{\bar{r}}{\delta_c} \quad u_\theta \equiv \frac{\bar{u}_\theta(\bar{r})}{\bar{u}_c} \quad (2)$$

This choice of reference length and velocity is ideally suited to model external swirl driven motions.

### B. Oseen-Lamb Vortex (1932)

The Oseen-Lamb vortex is a time-dependent line vortex that decays with the passage of time due to the presence of shear [23]. It constitutes a simple model of a viscous vortex that can be derived directly from the axisymmetric, incompressible, Navier-Stokes equations. The Oseen-Lamb vortex starts as a potential vortex in which  $\bar{u}_\theta(0,0) = 0$  is set to vanish initially along the axis of rotation. The subsequent radial decay may be captured in terms of the viscosity and total circulation  $\Gamma$ . The latter is taken to be the limiting value of vortex circulation as  $\bar{r} \rightarrow \infty$ . At the outset, one gets

$$\bar{u}_\theta(\bar{r}, t) = \frac{\Gamma}{2\pi\bar{r}} \left[ 1 - \exp\left(-\frac{\bar{r}^2}{4\nu t}\right) \right] = \frac{\Gamma}{2\pi\bar{r}} \left[ 1 - \exp\left(-\frac{\bar{r}^2}{\delta^2}\right) \right] \quad (3)$$

Being only subject to viscous diffusion, the characteristic radius increases with  $\delta = 2\sqrt{\nu t}$ . In fact, the maximum swirl velocity occurs at

$$\delta_c = \sqrt{-\frac{1}{2} - \text{pln}\left[-1, -\frac{1}{2}\exp\left(-\frac{1}{2}\right)\right]} \delta \approx 1.1209064\delta = 2.2418128\sqrt{\nu t} \quad (4)$$

which is offset by a mere 12% from  $\delta$ . The peak velocity diminishes with successive increases in time or viscosity, being inversely proportional to  $\sqrt{\nu t}$ ; it is given by

$$\bar{u}_c \equiv (\bar{u}_\theta)_{\max} = \frac{1 - \exp\left\{\frac{1}{2} + \text{pln}\left[-1, -\frac{1}{2}\exp\left(-\frac{1}{2}\right)\right]\right\}}{\sqrt{-\frac{1}{2} - \text{pln}\left[-1, -\frac{1}{2}\exp\left(-\frac{1}{2}\right)\right]}} \frac{\Gamma}{2\pi\delta} = 0.050784169 \frac{\Gamma}{\sqrt{\nu t}} \quad (5)$$

An alternative representation may be constructed in which the peak velocity is used in lieu of the total circulation; this manipulation yields

$$\frac{\bar{u}_\theta}{\bar{u}_c} = \frac{\sqrt{-\frac{1}{2} - \text{pln}\left[-1, -\frac{1}{2}\exp\left(-\frac{1}{2}\right)\right]}}{1 - \exp\left\{\frac{1}{2} + \text{pln}\left[-1, -\frac{1}{2}\exp\left(-\frac{1}{2}\right)\right]\right\}} \frac{\delta}{\bar{r}} \left[ 1 - \exp\left(-\frac{\bar{r}^2}{\delta^2}\right) \right] \approx 1.566974 \frac{\delta}{\bar{r}} \left[ 1 - \exp\left(-\frac{\bar{r}^2}{\delta^2}\right) \right] \quad (6)$$

When comparing theory and experiments, it should be borne in mind that the peak velocity occurs at  $\delta_c$  and that the more precise length scale for the problem is  $\delta_c \approx 1.1209\delta$  [24]. Using this more accurate characteristic length, Eq. (6) becomes

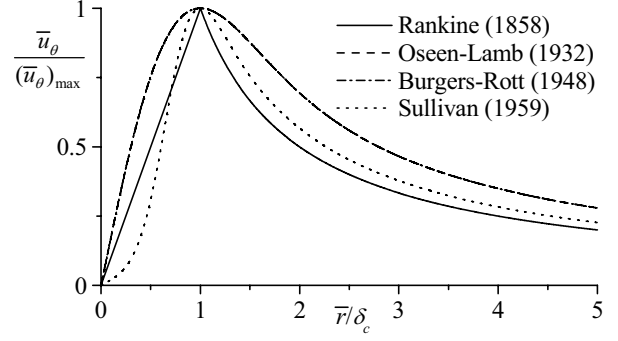


**Figure 4. Optimally rescaled tangential velocity profiles for the Rankine, Oseen-Lamb, Burgers-Rott, and Sullivan vortices. The unified normalization used here enables us to capture the strong similarities shared by these profiles.**

$$\begin{aligned}\frac{\bar{u}_\theta}{\bar{u}_c} &= \frac{1}{1 - \exp\left\{\frac{1}{2} + \text{pln}\left[-1, -\frac{1}{2}\exp\left(-\frac{1}{2}\right)\right]\right\}} \frac{\delta_c}{\bar{r}} \left[ 1 - \exp\left\{\left\{\frac{1}{2} + \text{pln}\left[-1, -\frac{1}{2}\exp\left(-\frac{1}{2}\right)\right]\right\} \frac{\bar{r}^2}{\delta_c^2}\right\}\right] \\ &\approx 1.39795255 \frac{\delta_c}{\bar{r}} \left[ 1 - \exp\left(-1.25643121 \frac{\bar{r}^2}{\delta_c^2}\right)\right]\end{aligned}\quad (7)$$

We hence reproduce Batchelor's laminar  $q$ -vortex solution (1964) which is plotted in Fig. 4 alongside Rankine's. The dimensionless and portable form of the Oseen-Lamb vortex emerges, namely,

$$u_\theta = \frac{K}{r} \left[ 1 - \exp(-\alpha r^2) \right] \quad (8)$$

where

$$\begin{cases} K = \frac{1}{1 - \exp\left\{\frac{1}{2} + \text{pln}\left[-1, -\frac{1}{2}\exp\left(-\frac{1}{2}\right)\right]\right\}} \approx 1.39795255 \\ \alpha = -\frac{1}{2} - \text{pln}\left[-1, -\frac{1}{2}\exp\left(-\frac{1}{2}\right)\right] \approx 1.25643121 \end{cases} \quad (9)$$

The origin and exact values of the classic constants,  $K$  and  $\alpha$ , are hereby unraveled.

### C. Burgers-Rott Vortex (1948)

The Burgers-Rott vortex is another exact solution to the Navier-Stokes equations. Unlike the Rankine model, it disposes of both axial and radial velocity components and can occur naturally given large convective atmospheric conditions. This added feature may be attributed to the suction parameter  $a$  which provides the freedom to model suction driven axial flows such as those observed in thunderstorms. Interestingly, as the suction parameter increases, the profile reduces to the Rankine approximation. Its mathematical basis is given by

$$\bar{u}_\theta(\bar{r}) = \frac{\Gamma}{2\pi\bar{r}} \left[ 1 - \exp\left(-\frac{\bar{r}^2}{2\nu/a}\right) \right] = \frac{\Gamma}{2\pi\bar{r}} \left[ 1 - \exp\left(-\frac{\bar{r}^2}{\delta^2}\right) \right] \quad (10)$$

where  $\delta = \sqrt{2\nu/a}$ . Clearly, when the radius is normalized by  $\delta$ , this profile becomes identical to the Oseen-Lamb expression. Both are superimposed in Fig. 4. Based on Eq. (5), the peak swirl can be calculated to be

$$\bar{u}_c = \frac{1 - \exp\left\{\frac{1}{2} + \text{pln}\left[-1, -\frac{1}{2}\exp\left(-\frac{1}{2}\right)\right]\right\}}{\sqrt{-\frac{1}{2} - \text{pln}\left[-1, -\frac{1}{2}\exp\left(-\frac{1}{2}\right)\right]}} \frac{\Gamma}{2\pi\delta} = 0.638172686 \frac{\Gamma}{2\pi\delta} = 0.07181966 \frac{\Gamma}{\sqrt{\nu/a}} \quad (11)$$

It should also be noted that both the Burgers-Rott and Oseen-Lamb vortices are axisymmetric Gaussian solutions of the incompressible Navier-Stokes equations. Both can be expressed as

$$\bar{u}_\theta = \Gamma G\left(\frac{\bar{r}}{\delta}\right); \quad G(x) = \frac{1}{4\pi} e^{-\frac{1}{4}x^2} \quad (12)$$

where  $G(x)$  is the normalized Gaussian function, and  $(\Gamma, \delta)$  denote their circulation and core characteristic scale. Despite their simplicity, these solutions continue to receive attention. Examples abound and one may cite those by Schmid and Rossi [25], Pérez-Saborid et al. [26], Eloy and Le Dizès [27], Alekseenko et al. [24], and Devenport et al. [28]. In several experiments, empirical relations are used based on Eq. (10), specifically,

$$\bar{u}_\theta = \frac{K}{2\pi\bar{r}} \left[ 1 - \exp\left(-\frac{\bar{r}^2}{\delta^2}\right) \right]; \quad u_z = W_1 + W_2 \exp\left(-\frac{\bar{r}^2}{\delta^2}\right) \quad (13)$$

where  $K, \delta, W_1$ , and  $W_2$  are constants that are determined empirically (see Leibovich [11,12], Faler and Leibovich [29], and Escudier [30]). Several other solutions are derived in similar context and described by Long [31], Alekseenko et al. [24], and others.

## III. Bidirectional Solutions

Solutions that represent bidirectional vortex motions are much less common in the literature. Here we consider those by Sullivan [32], Bloor and Ingham [33], and Vyas and Majdalani [34].

### A. Sullivan's Vortex (1959)

Sullivan's vortex is an exact viscous solution to the Navier-Stokes equations in an unbounded domain [32]. This profile corresponds to a two-cell structure; its inner cell comprises a region where fluid is in constant descent and then flows outwardly to rejoin a separate flow converging radially. This vortex captures physical mechanisms exhibiting a distinct inner downflow. Its integral representation consists of

$$\begin{cases} \bar{u}_\theta(\bar{r}) = \frac{\Gamma}{2\pi\bar{r}} \frac{1}{H(\infty)} H\left(\frac{\bar{r}^2}{2\nu/a}\right) = \frac{\Gamma}{2\pi\bar{r}} \frac{1}{H(\infty)} H\left(\frac{\bar{r}^2}{\delta^2}\right) \\ H(x) = \int_0^x e^{f(t)} dt; \quad f(t) = -t + 3 \int_0^t (1 - e^{-y}) \frac{dy}{y} \end{cases} \quad (14)$$

Note that the radial and axial velocity companions are given by

$$\begin{cases} \bar{u}_r(\bar{r}) = -a\bar{r} + \frac{6\nu}{\bar{r}} \left[ 1 - \exp\left(-\frac{\bar{r}^2}{\delta^2}\right) \right] \\ \bar{u}_r(\bar{r}, \bar{z}) = 2a\bar{z} \left[ 1 - 3 \exp\left(-\frac{\bar{r}^2}{\delta^2}\right) \right] \end{cases} \quad (15)$$

where  $\delta = \sqrt{2\nu/a}$ ;  $a$  is the suction strength and  $\nu$  is the viscosity dominated by the eddy viscosity. At first glance, the integral  $f(t)$  in Eq. (14) may appear to diverge. However, as the function is integrated, its contribution becomes negligible past a radial position corresponding to  $x = 10$ . For this reason, we see a strong resemblance in the tail region to that of a Rankine vortex. The peak circumferential velocity will occur when  $\bar{u}'_\theta(\bar{r}) = 0$  or

$$2(\bar{r}/\delta)^8 e^{3\mathcal{E} - \bar{r}^2 + 3\gamma(0, \bar{r}^2/\delta^2)} - \int_0^{\bar{r}^2/\delta^2} \exp\{-t + 3[\mathcal{E} + \gamma(0, t) + \ln(t)]\} dt = 0; \quad \delta_c = 2.49761606\delta \quad (16)$$

where  $\mathcal{E} \approx 0.57721566$  is Euler's gamma constant and  $\gamma$  is Euler's gamma function. A rescaled representation of Sullivan's vortex can be achieved using

$$\bar{u}_c = \frac{\Gamma}{2\pi\delta_c} \frac{1}{H(\infty)} H\left(\frac{\delta_c^2}{\delta^2}\right) \approx 0.0567688 \frac{\Gamma}{\delta} = 0.0401416 \frac{\Gamma}{\sqrt{\nu/a}} \quad (17)$$

and so,

$$\bar{u}_\theta = \frac{\Gamma}{2\pi\bar{r}} \frac{1}{H(\infty)} H\left(\frac{\bar{r}^2}{2\nu/a}\right) = \frac{2.497616}{2\pi\bar{r}} \frac{\Gamma}{H(\infty)} H\left(6.23809 \frac{\bar{r}^2}{\delta_c^2}\right) \quad (18)$$

Subsequent normalization by the maximum velocity yields

$$u_\theta = \frac{\bar{u}_\theta}{\bar{u}_c} = \frac{1}{H(6.23809)} \frac{\delta_c}{\bar{r}} H\left(6.23809 \frac{\bar{r}^2}{\delta_c^2}\right) \approx \frac{0.0298902}{r} H(6.23809r^2) \quad (19)$$

One may note the similarities among the foregoing solutions as depicted in Fig. 4.

### B. Bloor-Ingham Vortex (1987)

Bloor and Ingham's vortex [33] is an exact inviscid solution to Euler's equations in a confined, conical domain. Its advancement is intended to be an improvement over the Polhausen technique used earlier by the authors in the context of modeling cyclone separators [35]. Although their initial results agreed with Kelsall's experimental data [36], their model was not sensitive to variations in inlet flow conditions. In seeking a refined model, Bloor and Ingham [33] took the mean flow vorticity to be inversely proportional to the distance from their chamber axis and introduced some careful assumptions regarding the position and distribution of the inlet source. This enabled them to solve the inviscid Bragg-Hawthorne equation in spherical coordinates. Using our nomenclature and coordinates shown in Fig. 5b, one may anchor the origin of the spherical reference frame at the apex of the cone. Accordingly, Bloor and Ingham's vortex may be expressed as

$$\begin{aligned} \psi &= \frac{\bar{\psi}}{(Q_i/2\pi)} = \sigma R^2 \left\{ \left[ \csc^2 \alpha + \ln\left(\frac{1}{2} \tan \alpha\right) - \csc \alpha \cot \alpha \right] \sin^2 \phi - \sin^2 \phi \ln\left(\frac{1}{2} \tan \phi\right) + \cos \phi - 1 \right\} \\ &= \sigma r^2 \left\{ \csc^2 \alpha + \ln\left(\frac{1}{2} \tan \alpha\right) - \csc \alpha \cot \alpha - \ln\left(\frac{1}{2} \tan \phi\right) + \csc \phi \cot \phi - \csc^2 \phi \right\} \end{aligned} \quad (20)$$



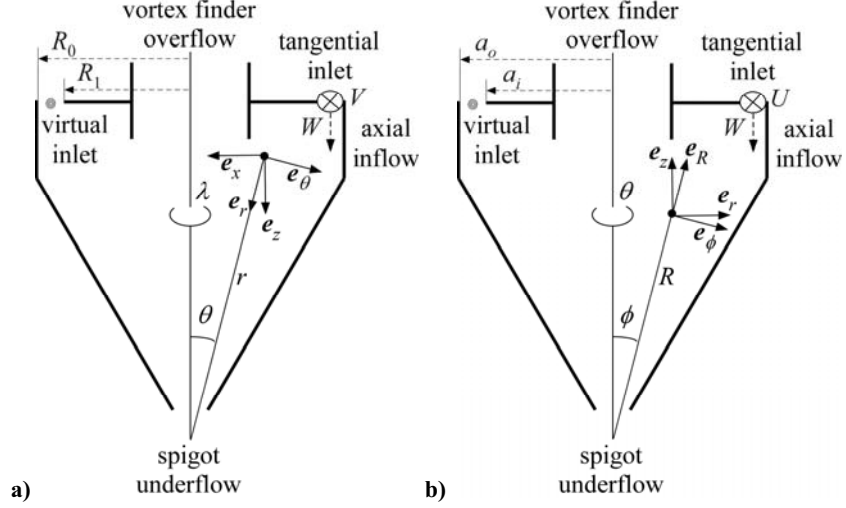


**Figure 5. Conical geometry and spherical coordinates used by a) Bloor and Ingham(1987) and b) corresponding variables and directional unit vectors used here.**

where the volume flow rate through the cyclone is  $\bar{Q}_i = \pi W(a_o^2 - a_i^2)$  and the overbar, as usual, denotes dimensional quantities. In Fig. 5,  $U$  is the average swirl velocity at entry and  $W$  is the average axial velocity component perpendicular to the lid. Assuming that axial injection from the top occurs at a uniform speed of  $W$  through a virtual opening,  $a_i < \bar{r} < a_o$ , neither  $W$  nor  $a_i$  are known at the outset because “they depend on the way in which the three-dimensional flow in the cylindrical section of the cyclone develops into the axially symmetric flow.” Unlike external flows in which the radial distance to the peak swirl velocity is taken to be the characteristic length, it is convenient to normalize radial and axial coordinates by  $a_o \equiv a$ ; the dimensionless parameter  $\sigma$  is given by

$$\sigma = \frac{\pi a_o^2 U^2}{\bar{Q}_i W} = \frac{U^2 / W^2}{(1 - a_i^2 / a_o^2)} \quad (21)$$

This can be obtained from Eq. (25) in [33]. The spherical solution comprises

$$u_R = \frac{\bar{u}_R}{(\bar{Q}_i / 2\pi a^2)} = 2\sigma \left[ \csc^2 \alpha + \ln\left(\frac{1}{2} \tan \alpha\right) - \csc \alpha \cot \alpha \right] \cos \phi - 2\sigma \left[ \cos \phi \ln\left(\frac{1}{2} \tan \phi\right) \right] \quad (22)$$

$$u_\phi = \frac{\bar{u}_\phi}{(\bar{Q}_i / 2\pi a^2)} = \frac{2\psi}{\sin 2\phi} \quad (23)$$

$$u_\theta = \frac{\bar{u}_\theta}{U} = \frac{1}{r} \sqrt{1 - \frac{\bar{Q}_i^2 \sigma \psi}{\pi^2 a^2 U^2}} \quad (24)$$

It is valid for  $0 < r < 1$  and becomes singular along the axis of the cyclone. When reverting back to cylindrical coordinates, one may use

$$\begin{cases} u_r = u_R \sin \phi - u_\phi \cos \phi \\ u_z = u_R \cos \phi + u_\phi \sin \phi \end{cases} \quad (25)$$

Note that the tangential velocity is normalized differently from the rest, being referenced to the average tangential velocity at entry. For small divergence angles of the conical chamber, one recovers

$$\psi = -\sigma r^2 \phi^2 \ln\left(\frac{\phi}{\alpha}\right) \csc^2 \phi \quad (26)$$

$$u_z = -\sigma \left[ 2(\theta + 1) \ln\left(\frac{\phi}{\alpha}\right) + 1 \right] \quad (27)$$

### C. Vyas-Majdalani Vortex (2003)

The Vyas-Majdalani vortex is an exact inviscid solution to Euler's equations derived in a confined, cylindrical domain. It is obtained using the vorticity-stream function approach and a novel technique introduced by Vyas, Majdalani and Chiaverini [37], and later refined by Vyas and Majdalani [34]. This technique is extended to spherical geometry by Majdalani and Rienstra [38] wherein the existence of additional exact solutions is demonstrated. The Vyas-Majdalani vortex shares similar features to those associated

with Bloor and Ingham's, including the inviscid singularity at the origin. However, it is not limited to the assumptions made previously, such as the requirement on the vorticity to remain inversely proportional to the radial distance throughout the chamber. The singularity at the origin is a known characteristic of inviscidly swirling motions and adds some reassurance to the result furnished in [34]; the singularity can actually be overcome by regularizing the tangential momentum equation before applying matched-asymptotic expansions [39]. Another interesting outcome of the inviscid model stems from its ability to predict the existence of multiple mantles in a cylindrical cyclone, as shown in a companion paper by Vyas, Majdalani and Chiaverini [8]. What was considered to be unlikely at first was confirmed, that same year, through the extensive laboratory and numerical experiments carried out independently by Anderson et al. [40].

In order to capture the sidewall boundary layers, Vyas and Majdalani have rescaled the tangential momentum equation and constructed a composite solution for the swirl velocity. This is an essential first step for a variety of reasons. Their approximation for  $u_\theta$  remains uniformly valid from the core to the sidewall, inclusively [41]. Along similar lines, Batterson and Majdalani [42] have rescaled the axial and radial momentum equations and provided an improved rotational, incompressible, steady-state solution for the problem at hand. The no slip condition is thus observed in all three directions. Parallel efforts have been carried out by Maicke and Majdalani [43] for the purpose of producing a fully compressible approximation. Theirs is based on a Rayleigh-Janzen expansion that has proved successful in the treatment of compressible Taylor and Culick profiles [44-46]. Such profiles are parameter-free, inviscid, rotational, and non-swirling; nonetheless, they are ubiquitously used and shown to be suitable models for the internal flowfield in solid rocket motors. In what follows, some of these developments are briefly described.

#### 1. Solution for the Inviscid Bidirectional Vortex

The mathematical model for the bidirectional vortex family of solutions is illustrated in Fig. 6. The idealized tube has length  $L$  and radius  $a$ . The radius of the inner vortex is  $b$ , which coincides with the radius of the exiting stream (i.e., the outflow). Initially,  $\bar{r}$  and  $\bar{z}$  are used to denote the radial and axial coordinates. The outflow fraction of the radius is given by  $\beta = b/a$  and the chamber's aspect ratio is taken to be  $l = L/a$ .

As in the case of the Bloor-Ingham vortex, a virtual opening in the sidewall is assumed to exist, thus permitting tangential fluid injection at an average speed of  $U$  across an inlet flow area of  $A_i$ . As listed in the Nomenclature, the inlet volumetric flow rate is  $\bar{Q}_i = UA_i$ . At this point, all spatial coordinates and velocities are normalized, consistently, by the radius  $a$  and the average tangential speed  $U$ . Given inviscid, rotational, incompressible, axisymmetric, and steady motion, Euler's equations reduce to

$$\nabla \cdot \mathbf{u} = 0; \quad \mathbf{u} \cdot \nabla \mathbf{u} = -\nabla p \quad (28)$$

In the process of reducing the number of dependent variables, one eliminates the pressure and introduces the vorticity transport equation,  $\nabla \times (\mathbf{u} \times \boldsymbol{\Omega}) = 0$ . One also introduces the Stokes stream function through the use of

$$u_r = -\frac{1}{r} \frac{\partial \psi}{\partial z}; \quad u_z = \frac{1}{r} \frac{\partial \psi}{\partial r} \quad (29)$$

so continuity is secured. The vorticity stream function will be satisfied, in turn, when a specific connection is found between mean flow vorticity and the stream function, specifically, when  $\Omega_\theta = rF(\psi)$ . Following standard practice, we choose  $F = C^2\psi$  and substitute into the vorticity equation. We retrieve the reduced form of the Bragg-Hawthorne equation, namely,

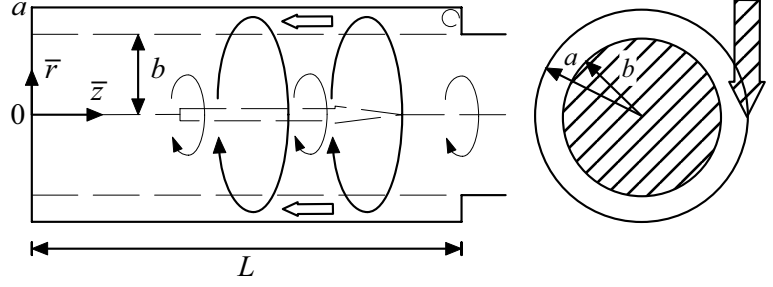


Figure 6. Sketch of the bidirectional vortex chamber and corresponding coordinate system before variables are normalized by the radius  $a$ .

$$r\Omega_\theta = \frac{1}{r} \frac{\partial \psi}{\partial r} - \frac{\partial^2 \psi}{\partial r^2} - \frac{\partial^2 \psi}{\partial z^2} \quad \text{or} \quad \frac{\partial^2 \psi}{\partial z^2} + \frac{\partial^2 \psi}{\partial r^2} - \frac{1}{r} \frac{\partial \psi}{\partial r} + C^2 r^2 \psi = 0 \quad (30)$$

At this juncture, separation of variables precipitates

$$\psi = (C_1 z + C_2) \left[ C_3 \sin\left(\frac{1}{2} C r^2\right) + C_4 \cos\left(\frac{1}{2} C r^2\right) \right] \quad (31)$$

This can be readily solved given a judicious assortment of boundary conditions. For the problem at hand, we have

- (a) tangential injection or  $u_\theta(l, l) = 1$  ;
- (b) no flow penetration at the headwall or  $u_z(r, 0) = 0$  ;
- (c) no asymmetry with respect to the centerline or  $u_r(0, z) = 0$  ;
- (d) no flow penetration at the sidewall or  $u_r(l, z) = 0$  ;
- (e) mass balance between inflow and outflow or  $Q_o = 2\pi \int_0^\beta u_z(r, l) r dr = Q_i$  .

Condition (a) can be readily used in conjunction with the conservation principle of angular momentum, given a frictionless fluid, to recover the free vortex  $u_\theta(r) = r^{-1}$ . The remaining conditions can be written in terms of the Stokes stream function and rearranged to produce

$$\begin{cases} z = 0 \rightarrow u_z = 0 \rightarrow \partial \psi / \partial r = 0 \\ r = 0 \rightarrow u_r = 0 \rightarrow \partial \psi / \partial z = 0 \\ r = l \rightarrow u_r = 0 \rightarrow \partial \psi / \partial z = 0 \\ z = l \rightarrow \int_0^{2\pi} \int_0^\beta (\partial \psi / \partial r) dr d\theta = Q_i \end{cases} \quad (32)$$

where  $Q_i = \bar{Q}_i / (Ua^2) = \sigma^{-1}$  is inversely proportional to the modified swirl number  $\sigma$ . The solution to Eq. (31) can be retrieved using the four requirements enumerated in Eq. (32). One recovers  $C = 2m\pi$  and

$$\begin{cases} \psi = \kappa z \sin(m\pi r^2) = \frac{1}{2\pi\sigma} \frac{z}{l} \sin(m\pi r^2) \\ \mathbf{u} = -\frac{\kappa}{r} \sin(m\pi r^2) \mathbf{e}_r + \frac{1}{r} \mathbf{e}_\theta + 2\pi\kappa z \cos(m\pi r^2) \mathbf{e}_z \end{cases} \quad (33)$$

where  $m$  represents the number of mantles, whereas  $\kappa$  and  $\sigma$  represent the dimensionless inflow and swirl parameters. These are determined from

$$\kappa = \frac{A_i}{2\pi aL} = \frac{1}{2\pi\sigma l} \quad \sigma = \frac{\sqrt{2}}{\pi} S = \frac{a^2}{A_i} \quad (34)$$

Note that  $\sigma$  emerges naturally in our work as a result of proper scaling. In relation to the standard swirl number  $S$  used by Gupta, Lilley and Syred [14], one gets  $S \approx 2.22144\sigma$ . This direct proportionality is, of course, gratifying. Another useful result is the theoretical determination of the mantle location which, according to Eq. (33), occurs at

$$r = \beta_{m,n} = \sqrt{(n - \frac{1}{2}) / m}, \quad n = 1, 2, 3, \dots, m \quad (35)$$

where  $n$  represents the  $n$ th internal mantle for a given reversal mode number  $m$  [8]. The most prevalent case corresponds to  $m = 1$  for which the mantle is predicted to occur at the vortex “rms” radius of  $\beta_{1,1} = \sqrt{2} / 2 \approx 0.707$ .

This value is compared in Table 1 to the two cases obtained in a cylindrical cyclone by Smith [47]. Note that our idealization is closer to the parameters used in Case II, thus explaining the closer agreement in the last column, with an average of 0.72. The combined average

**Table 1 Mantle locations according to Smith at MIT [47].**

Position	Case I inches	Case II inches	Case I normalized	Case II normalized
1	1.99	2.13	0.6633	0.7083
2	1.89	2.15	0.6300	0.7166
3	1.88	2.15	0.6266	0.7166
4	1.85	2.15	0.6166	0.7166
5	1.79	2.17	0.5966	0.7233
6	1.79	2.20	0.5966	0.7333
7	1.75	2.20	0.5833	0.7333
mean	1.85	2.16	0.6166	0.7211

**Table 2 Mantle locations vs. Anderson et al. [40] at UW.**

$\beta_{\text{exp}}$	$\beta_{\text{analytic}}$	$\beta_{\text{CFD}}$	$ \beta_{\text{analytic}} - \beta_{\text{exp}} $	$ \beta_{\text{CFD}} - \beta_{\text{exp}} $
0.296	0.354	0.305	0.058	0.009
0.594	0.612	0.385	0.018	0.209
0.803	0.791	0.787	0.012	0.016
0.955	0.935	1.000	0.020	0.045

obtained by Smith is 0.67 and may have been influenced by the presence of a vortex finder protruding into the chamber for the purpose of guiding the outflow. In the case of four mantles, the results so obtained are showcased in Table 2 versus experimental and numerical measurements obtained by Anderson et al. [40]. It is interesting that Eq. (35) agrees more closely with the experimental results than the numerical simulations. Nonetheless, the set of operating conditions that begets the onset of multiple mantles remains a subject of investigation and conjecture.

Before leaving this subject, it should be noted that, in what concerns the swirl number, it is generally defined as the ratio of tangential to axial momentum forces. Its scaling can vary from experiment to experiment, depending on the geometry and scaling used by the authors. For example, Hoekstra, Derksen, and van den Akker [48] define their swirl number as

$$S = \frac{\pi d_e D}{4 ab} = \frac{\pi (2b)(2a)}{4 A_i} = \frac{\pi \beta a^2}{A_i} \quad (36)$$

where “ $d_e$ ” is the diameter of the vortex finder (exit tube), “ $ab$ ” is the tangential inlet area of the cyclone (here, we use  $A_i$  instead), and “ $D$ ” is the diameter of the cyclone (here, we use  $2a$ ). It can be easily shown that Eq. (36) reduces to Eq. (34). Conversely, for a combustor with swirl vanes, Lilley [13] defines the corresponding swirl number to be

$$S = \frac{2}{3} \left[ \frac{1 - (d_h/d)^3}{1 - (d_h/d)^2} \right] \tan \phi \quad (37)$$

where “ $d$ ” and “ $d_h$ ” denote the nozzle diameter and hub diameter of the vanes, and “ $\phi$ ” stands for the vane angle.

## 2. Solution for the Tangential Boundary Layers

The presence of viscosity at the core and sidewall need to be properly accounted for to capture the forced vortex and near-wall decay. The approach we take is to reconsider the tangential momentum equation with viscosity [49].

The basic solution of this set is expressible by

$$\mathbf{u} = -\kappa \frac{\sin(\pi r^2)}{r} \mathbf{e}_r + u_\theta(r) \mathbf{e}_\theta + 2\pi \kappa z \cos(\pi r^2) \mathbf{e}_z; \quad \kappa \equiv \frac{Q_i}{2\pi l} = \frac{A_i}{2\pi aL} = \frac{1}{2\pi \sigma l} \quad (38)$$

where  $u_\theta = r^{-1}$  is deficient near  $r=0$  and does not observe the velocity-adherence requirement at the sidewall. Both problems stem from the absence of viscosity in the leading order, basic model. To overcome these issues, the  $\theta$  – momentum equation is reconsidered with second-order viscous terms, namely,

$$u_r \frac{\partial u_\theta}{\partial r} + \frac{u_r u_\theta}{r} = \frac{1}{Re} \left( \nabla^2 u_\theta - \frac{u_\theta}{r^2} \right) = \frac{1}{Re} \frac{\partial}{\partial r} \left[ \frac{1}{r} \frac{\partial (ru_\theta)}{\partial r} \right]; \quad Re \equiv \frac{Ua}{\nu} \quad (39)$$

where  $Re$  is the mean flow Reynolds number. Being axially independent, Eq. (39) reduces to

$$u_r \frac{du_\theta}{dr} + \frac{u_r u_\theta}{r} = \varepsilon \frac{d}{dr} \left[ \frac{1}{r} \frac{d}{dr} (ru_\theta) \right]; \quad \varepsilon \equiv \frac{1}{Re} \quad (40)$$

This can be quickly transformed into

$$\frac{\varepsilon}{\kappa} \frac{d^2 \xi}{d\eta^2} + \frac{\sin \eta}{2\eta} \frac{d\xi}{d\eta} = 0; \quad \xi \equiv ru_\theta; \quad \eta \equiv \pi r^2 \quad (41)$$

where  $\kappa \sim 10^{-3} - 10^{-2}$ . To make further headway, the boundary layers near the core and sidewall must be identified (see Fig. 7). But first, we note that the outer solution may be restored from Eq. (41) by setting  $\varepsilon = 0$ . One recovers  $\xi^{(o)} = \bar{C}$ , where  $(o)$  denotes an outer approximation and  $\bar{C}$  is a constant.

## Inner, Near Core Approximation

In order to bring the swirl velocity to zero along the chamber axis, one must introduce the slow variable

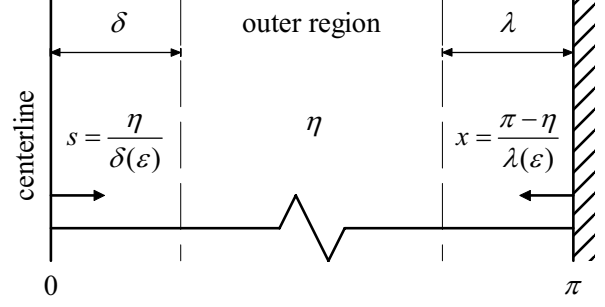


**Figure 7. Presence of endpoint boundary layers affecting the tangential velocity and causing it to vanish both at the centerline (thus giving rise to a forced vortex) and the sidewall (in fulfillment of no slip).**

$$s \equiv \frac{\eta}{\delta(\varepsilon)} \quad (42)$$

A balance between diffusion and convection near the core leads to the distinguished limit of  $\delta \sim \varepsilon / \kappa$ . The core boundary layer equation becomes exceedingly simple, namely,

$$\frac{d^2 \xi^{(i)}}{ds^2} + \frac{1}{2} \frac{d\xi^{(i)}}{ds} = 0; \quad \begin{cases} r=0, s=0, \xi^{(i)}=0 \\ r \rightarrow 1, s \rightarrow \infty, \xi^{(i)} = \xi^{(o)} \end{cases} \quad (43)$$

where the superscript stands for the inner, near-core approximation. Using a series of the form  $\xi^{(i)} = \xi_0^{(i)} + \delta \xi_1^{(i)} + \dots$  one retrieves

$$\xi^{(i)} = C_0 (e^{-\frac{1}{2}s} - 1) \quad (44)$$

Then using Prandtl's matching principle, we deduce  $C_0 = -\bar{C}$ . The last constant may be obtained from the downstream condition of a tangentially injected fluid. A composite inner solution is hence determined,

$$\xi^{(ci)} = \frac{1 - e^{-\frac{1}{4}Vr^2}}{1 - e^{-\frac{1}{4}V}} \quad \text{or} \quad u_\theta^{(ci)} = \frac{1}{r} \left( \frac{1 - e^{-\frac{1}{4}Vr^2}}{1 - e^{-\frac{1}{4}V}} \right) \quad (45)$$

where  $V$  is the vortex Reynolds number that appears in the problem. This parameter combines the viscous Reynolds number, the swirl number and the geometric aspect ratio:

$$V \equiv \frac{2\pi\kappa}{\varepsilon} = \frac{1}{\varepsilon\sigma l} = \frac{Re}{\sigma} \frac{a}{L} = \frac{\bar{Q}_i}{Lv} \quad (46)$$

It may be interesting to note the qualitative resemblance between Eq. (46) and the vortex Reynolds number encountered in two cell swirling motion such as Sullivan's vortex [32]; Sullivan's control parameter is found to be proportional to the flow circulation at infinity and the reciprocal of the kinematic viscosity.

The composite inner approximation is identical to the solution presented by Vyas, Majdalani and Chiaverini [39] Note that as  $\varepsilon \rightarrow 0$ ,  $V \rightarrow \infty$ , and  $u_\theta^{(ci)} \rightarrow r^{-1}$ ; forthwith, the swirl velocity associated with a free vortex is restored. Conversely, as  $r \rightarrow 0$  at fixed  $\varepsilon$ , one can expand Eq. (45) into

$$u_\theta^{(ci)} = \frac{rV(1 - \frac{1}{8}Vr^2 + \frac{1}{96}V^2r^4 + \dots)}{4(1 - e^{-\frac{1}{4}V})} = \frac{rV}{4} + O(r^3) \quad (47)$$

This expansion unravels the forced vortex relation,  $u_\theta^{(ci)} \sim \omega r$ , where  $\omega \sim \frac{1}{4}V$ ,  $\omega$  being the angular speed of the core that is rotating as a rigid body about the chamber axis.

### Inner, Sidewall Approximation

In similar fashion, the sidewall boundary layer may be captured after rescaling the thin region near the wall via

$$x \equiv \frac{\pi - \eta}{\lambda(\varepsilon)} \quad (48)$$

Here  $\lambda$  refers to the thickness of the wall tangential boundary layer. Using (w) to denote a wall solution, Eq. (41) may be rearranged, expanded, and reduced to

$$\frac{d^2 \xi^{(w)}}{dx^2} + \frac{1}{2} \left( \frac{1}{6} \pi^2 - 1 \right) \frac{d\xi^{(w)}}{dx} = 0; \quad \begin{cases} r=1, x=0, \xi^{(w)}=0 \\ r \rightarrow 0, x \rightarrow \infty, \xi^{(w)} = \xi^{(ci)} \end{cases} \quad (49)$$

where  $\lambda \equiv \varepsilon / \kappa$  is taken to be the distinguished limit. Corresponding boundary conditions consist of the no slip at the wall and blending with the composite inner solution in the outer domain. Following similar ideas of matching, the sidewall approximation may be obtained,

$$\xi^{(w)}(r) = \frac{1 - e^{-\frac{1}{4}(\frac{1}{6}\pi^2 - 1)V(1-r^2)}}{1 - e^{-\frac{1}{4}(\frac{1}{6}\pi^2 - 1)V}} \quad \text{or} \quad u_\theta^{(w)} = \frac{1}{r} \left[ \frac{1 - e^{-\frac{1}{4}(\frac{1}{6}\pi^2 - 1)V(1-r^2)}}{1 - e^{-\frac{1}{4}(\frac{1}{6}\pi^2 - 1)V}} \right] \quad (50)$$

The validity of Eq. (50) is restricted to the region adjacent to the wall. As  $r \rightarrow 0$ , the outer solution is regained.

### Composite, Uniformly Valid Approximation

Using the classic ideas of composite expansions, a uniformly valid solution may be arrived at from the combination of wall and composite inner solutions. The result is

$$u_\theta = \begin{cases} \frac{1}{r} \left[ \frac{1 - e^{-\frac{1}{4}Vr^2}}{1 - e^{-\frac{1}{4}V}} + \frac{1 - e^{-\frac{1}{4}(\frac{1}{6}\pi^2 - 1)V(1-r^2)}}{1 - e^{-\frac{1}{4}(\frac{1}{6}\pi^2 - 1)V}} - 1 \right] \approx \frac{1}{r} \left[ 1 - e^{-\frac{1}{4}Vr^2} - e^{-\frac{1}{4}(\frac{1}{6}\pi^2 - 1)V(1-r^2)} \right]; & 0 < z < l \\ \frac{1}{r} \left( \frac{1 - e^{-\frac{1}{4}Vr^2}}{1 - e^{-\frac{1}{4}V}} \right) \approx \frac{1}{r} \left( 1 - e^{-\frac{1}{4}Vr^2} \right); & z = l \quad (\text{tangential injection at entry}) \end{cases} \quad (51)$$

The swirl velocity is hence made non-singular and adjusted to satisfy the no slip condition at the wall. Its behavior is illustrated in Figs. 8 and 9. Other important flow ingredients are summarized in Table 3.

As shown in Fig. 8, the tangential component of the velocity starts from zero at the wall and then increases rapidly to merge with the outer flowfield within a characteristic distance  $\delta_w$ . It continues to increase until reaching a maximum value that delimits the envelope inside of which viscous forces become dominant. After passing through this maximum  $(u_\theta)_{\max}$ , the swirl velocity depreciates, within a radius  $\delta_c$ , until it reaches zero at the chamber axis. The plot of  $u_\theta$  in Fig. 8 is given at three vortex Reynolds numbers of  $10^2$ ,  $10^3$ , and  $10^4$ .

As shown in Fig. 8a and its inset, the radius of the core vortex  $\delta_c$  expands with successive increases in viscosity. It is largest at the smallest value of  $V$ . As the vortex Reynolds number is increased to  $10^4$ , the point of maximum swirl draws nearer to the core. This behavior is accompanied by an increase in the magnitude of  $(u_\theta)_{\max}$ . With further increases in the vortex Reynolds number, it is clear that  $u_\theta$  approaches the inviscid limit.

In the close proximity of the sidewall, Fig. 8b illustrates the rapid damping that the swirl velocity undergoes. The wall tangential boundary layer  $\delta_w$  exhibits a similar dependence on viscosity. Its thickness increases when the vortex Reynolds number is decreased. The patterns of the rapidly decaying curves appear to be in agreement with experimental measurements acquired by Hu et al. [52]. They also agree with both CFD and LDV predictions obtained by Hoekstra, Derksen and Van den Akker [48].

In the interest of validating the shape predicted by the present solution, comparisons are made in Fig. 9 using numerical simulations and experimental measurements obtained, respectively, from Murray et al. [50], and Rom,

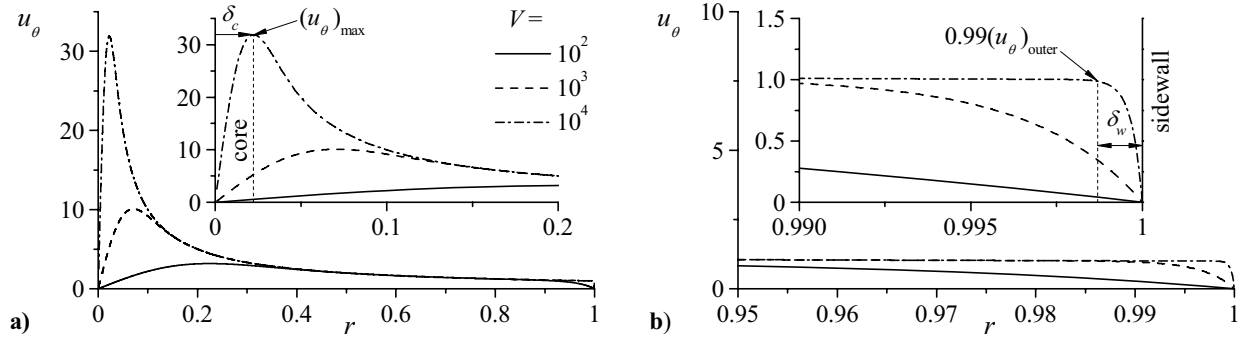


**Figure 8.** Swirl velocity versus  $V = \bar{Q}_i / (Lv)$  illustrating the sensitivity of the boundary layer thickness near a) the core and b) the sidewall.

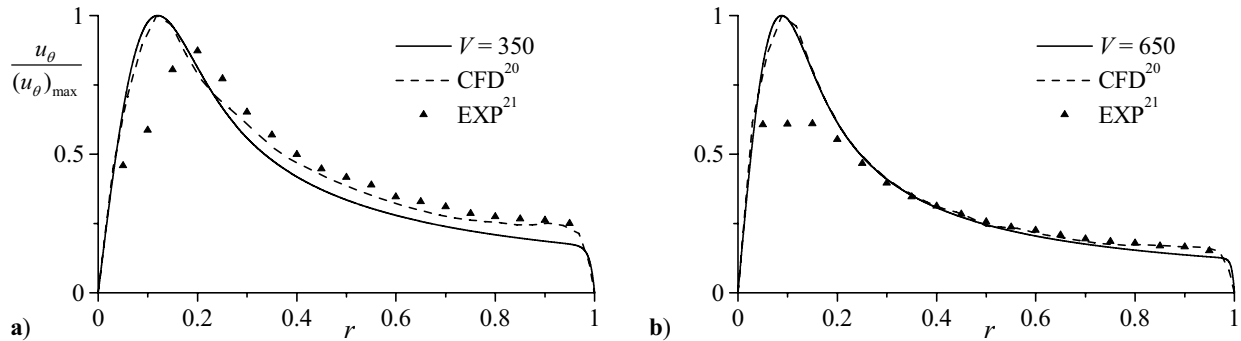


**Figure 9.** Analytical swirl velocity  $u_\theta^{(c)}$  versus computational and experimental predictions from Murray et al. [50] and Rom, Anderson and Chiaverini [51]. Our solutions are shown at two vortex Reynolds numbers corresponding to a) 350, and b) 650.

Anderson and Chiaverini (cf. Fig. 18) [51]. The numerical data is generated using KIVA, a three-dimensional, finite-volume solver that can handle multiphase, multicomponent, chemically reacting flows. The code is based on a staggered, Arbitrary Lagrangian Eulerian (ALE) technique. The measurements are acquired through Particle Image Velocimetry (PIV) and an experimental apparatus that is elaborately described by Anderson et al. [40,51]. In both parts of Fig. 9, numerical and analytical shape predictions show substantial agreement at the estimated vortex Reynolds numbers; furthermore, they are corroborated by actual experimental measurements, especially in the outer and sidewall regions.

As the core is approached, the experimental velocity tapers off, falling short of the maximum theoretical values projected by computations and asymptotics. The reduced fidelity of the PIV technique in the vicinity of the forced vortex region is not surprising; it may be attributed to the intensification of viscous drag on seeded particles. Similar trends are depicted in the RSM data and rich LDV measurements taken recently by Hu et al. (cf. Fig. 8 in [52]). Their LDV data acquisition system also deteriorates in the core neighborhood. Several arguments could be offered as plausible explanations. While approaching  $r = \delta_c$  from the outer domain, particle drag increases and the swirl velocity becomes quite high relative to the radial velocity; it becomes difficult for the particles to follow the flow or for the experimenter to achieve good seeding concentrations. To increase the precision of measurements, it is essential to use correlated particle pairs from two pulsed laser planes.

#### D. Batterson-Majdalani Vortex (2007)

The purpose of this solution is to achieve an approximation for the bidirectional vortex that satisfies no slip in all of its components [42]. It will seek to capture the boundary layers needed to bring both the axial and radial velocities to smoothly vanish along the sidewall. The required analysis is sketched below.

##### 1. Solution for the Axial Boundary Layer

The pertinent boundary layer equation can be derived according to Prandtl's order of magnitude reduction applied to the axisymmetric Navier-Stokes momentum equation [53]:

$$u_r \frac{\partial u_z}{\partial r} + u_z \frac{\partial u_z}{\partial z} = -\frac{\partial p}{\partial z} + \varepsilon \left( \frac{\partial^2 u_z}{\partial r^2} + \frac{1}{r} \frac{\partial u_z}{\partial r} \right) \quad (52)$$

This equation is subject to two conditions

$$\begin{cases} u_z(1, z) = 0 \\ \lim_{r \rightarrow 0} u_z(r, z) = u_z^{(o)} \end{cases} \quad (53)$$

where  $u_z^{(o)}$  represents the outer form that must be recovered by  $u_z(r, z)$  away from the walls. In the process, we extract the pressure gradient from the inviscid solution,  $\partial p / \partial z = -4\pi^2 \kappa^2 z$ . Moreover, an immediate simplification may be made as suggested by Conlisk [54]. By specifically stating that  $\partial / \partial r \gg \partial / \partial z$ , we are able to neglect derivatives with respect to the axial direction. This enables us to convert the partial differential equation (PDE) into an ordinary differential equation (ODE) that is valid at any fixed axial position. Lastly, the idea of successive approximations may be employed by injecting the radial outer solution into the boundary layer equation.

Applying these assumptions to Eq. (52) leads to the compacted form

$$\varepsilon \frac{1}{r} \frac{d}{dr} \left( r \frac{du_z}{dr} \right) + \frac{\kappa}{r} \sin(\pi r^2) \frac{du_z}{dr} = -4\pi^2 \kappa^2 z \quad (54)$$

A useful variable transformation found by Vyas and Majdalani [55] may be employed. We thus define  $\eta = \pi r^2$ . Upon substitution into Eq. (54) we retrieve

$$\varepsilon \left( \frac{d^2 u_z}{d\eta^2} + \frac{1}{\eta} \frac{du_z}{d\eta} \right) + \frac{\kappa}{2\eta} \sin(\eta) \frac{du_z}{d\eta} = -\frac{\pi \kappa^2 z}{\eta} \quad (55)$$

In order to more easily confront the rapid changes near the wall, we seek a scaling transformation appropriate of the boundary layer. We know that as  $r \rightarrow 1$ ;  $\eta \rightarrow \pi$ . We therefore select the stretched coordinate

$$s = \frac{\pi - \eta}{\delta}; \quad \eta = \pi - s\delta \quad (56)$$

This transformation leads to

$$\frac{\varepsilon}{\delta^2} \left( \frac{d^2 u_z}{ds^2} - \frac{\delta}{\pi - s\delta} \frac{du_z}{ds} \right) - \frac{\kappa \sin(\pi - s\delta)}{2\delta(\pi - s\delta)} \frac{du_z}{ds} = -\frac{4\pi\kappa^2 z}{\pi - s\delta} \quad (57)$$

Expanding the sine term leaves us with

$$\frac{\varepsilon}{\delta^2} \left( \frac{d^2 u_z}{ds^2} - \frac{\delta}{\pi - s\delta} \frac{du_z}{ds} \right) + \frac{\kappa}{2\delta} \left( \frac{\pi^2}{6} - 1 \right) \frac{du_z}{ds} = -\frac{4\pi\kappa^2 z}{\pi - s\delta} \quad (58)$$

As usual, the distinguished limit is found to be  $\delta \sim \varepsilon / \kappa$ . Upon substitution back into Eq. (58) we asymptotically reduce the equation to its final form

$$\frac{d^2 u_z}{ds^2} + \frac{1}{2} \left( \frac{\pi^2}{6} - 1 \right) \frac{du_z}{ds} = 0 \quad (59)$$

with the translated boundary conditions

$$\begin{cases} u_z(0, z) = 0 \\ \lim_{s \rightarrow \infty} u_z(s, z) = u_z^{(o)} \end{cases} \quad (60)$$

This equation captures the axial velocity profile *in the boundary layer at any given axial position*. Forthwith, Eq. (59) is satisfied by the function

$$u_z = u_z^{(o)} \left\{ 1 - \exp \left[ -\frac{1}{2} \left( \frac{\pi^2}{6} - 1 \right) s \right] \right\} \quad (61)$$

The outer approximation at any point is given by the inviscid solution  $u_z^{(o)} = 2\pi\kappa z \cos(\pi r^2)$ . Rewriting Eq. (61) in terms of the unscaled variables renders the final solution. One gets

$$u_z(r, z) = 2\pi\kappa z \cos(\pi r^2) \left[ 1 - e^{-\frac{1}{4}(\frac{1}{6}\pi^2 - 1)V(1-r^2)} \right] \quad (62)$$

where  $V = 2\pi\kappa / \varepsilon$  is the same vortex Reynolds number expressed in Eq. (46). We also note the symmetry between the axial boundary layer correction and that realized for the swirl velocity at the wall.

## 2. Solution for the Radial Boundary Layer

Corrections of this nature are typically disregarded if the inviscid velocity vanishes at the wall; however viscosity has a tempering effect on the curvature of the radial profile that will be investigated here. The reduction of the Navier-Stokes equations is more subtle because the viscous correction could be considered to be secondary. While Prandtl's method still applies, one must retain terms to the second order lest a meaningless outcome is engendered. The process requires starting with

$$\varepsilon \left( \frac{\partial^2 u_r}{\partial r^2} + \frac{1}{r} \frac{\partial u_r}{\partial r} - \frac{u_r}{r^2} \right) - u_r \frac{\partial u_r}{\partial r} + \frac{u_\theta^2}{r} - u_z \frac{\partial u_r}{\partial z} = \frac{\partial p}{\partial r} \quad (63)$$

which is subject to

$$\begin{cases} u_r(1) = 0 \\ \lim_{r \rightarrow 0} u_r(r) = u_r^{(o)} \end{cases} \quad (64)$$

By assuming that radial changes are more significant than axial ones, we eliminate all axial derivatives and take the pressure gradient calculated from the inviscid solution obtained in [34],

$$\frac{\partial p}{\partial r} = \frac{\kappa^2}{r^3} \sin^2(\pi r^2) \left[ 1 - 2\pi r^2 \cot(\pi r^2) \right] + \frac{1}{r^3} \quad (65)$$

We recognize that this term becomes  $O(\kappa^2)$  near the wall due to some cancellation with the  $u_\theta^2 / r$  term. Then just as before, we inject the inviscid solution into the boundary layer equation. Rewriting Eq. (63) gives

$$\varepsilon \left[ \frac{1}{r} \frac{d}{dr} \left( r \frac{du_r}{dr} \right) + \frac{\kappa}{r^3} \sin(\pi r^2) \right] + \frac{\kappa}{r} \sin(\pi r^2) \frac{du_r}{dr} = O \left[ \frac{\kappa^2}{r^3} \sin^2(\pi r^2) \right] \quad (66)$$

The transformation  $\eta = \pi r^2$  follows. With careful substitution and factorization of Eq. (66), we get

$$\varepsilon \left[ \frac{d^2 u_r}{d\eta^2} + \frac{1}{\eta} \frac{du_r}{d\eta} + \frac{\kappa \sqrt{\pi}}{4\eta^{5/2}} \sin(\eta) \right] + \frac{\kappa}{2\eta} \sin(\eta) \frac{du_r}{d\eta} = O \left[ \frac{\kappa^2}{r^3} \sin^2(\pi r^2) \right] \quad (67)$$



The sidewall variable transformation  $s = (\pi - \eta) / \delta$  can thus be applied along with the sine expansion; the radial equation becomes

$$\frac{\varepsilon}{\delta^2} \left[ \frac{d^2 u_r}{ds^2} - \frac{\delta}{\pi - s\delta} \frac{du_r}{ds} + \frac{\delta^2 \kappa \sqrt{\pi}}{4(\pi - s\delta)^{5/2}} \sin(\pi - s\delta) \right] + \frac{\kappa}{2\delta} \left( \frac{\pi^2}{6} - 1 \right) \frac{du_r}{ds} \approx 0 \quad (68)$$

where  $\delta \sim \varepsilon / \kappa$  re-emerges. Reinserting the distinguished limit into Eq. (68) we can reveal the following form

$$\frac{d^2 u_r}{ds^2} + \frac{1}{2} \left( \frac{\pi^2}{6} - 1 \right) \frac{du_r}{ds} = 0 \quad \text{or} \quad \frac{d^2 \xi_r}{ds^2} + \left( \frac{\pi^2}{6} - 1 \right) \frac{d\xi_r}{ds} = 0 \quad (69)$$

Note that we introduce  $\xi_r = ru_r / \sin(\pi r^2)$ . Boundary conditions follow, namely,

$$\begin{cases} u_r(0) = 0 \\ \lim_{s \rightarrow \infty} u_r(s) = u_r^{(o)} \end{cases} \quad \text{or} \quad \begin{cases} \xi_r(0) = 0 \\ \lim_{s \rightarrow \infty} \xi_r(s) = \xi_r^{(0)} = -\kappa \end{cases} \quad (70)$$

The solution is readily found to be

$$u_r(r, z) = -\frac{\kappa}{r} \sin(\pi r^2) \left[ 1 - e^{-\frac{1}{2}(\frac{1}{6}\pi^2 - 1)V(1-r^2)} \right] \quad (71)$$

The new solutions resolve the viscous corrections near the wall. Figure 10a illustrates the inviscid solution with respect to given axial positions while Fig. 10b illustrates the strong dependence of the boundary layer on the vortex Reynolds number. Since both corrections possess the same basic form, we can conclude that the boundary layer thickness will be similar in both directions. Graphically, the axial dependence on the vortex Reynolds number appears to be more significant than in the radial case. In both coordinate directions, as  $V \rightarrow \infty$  the inviscid solution is restored. Inversely, as  $V \rightarrow 0$  the solution vanishes, as in the case of zero mean flow velocity.

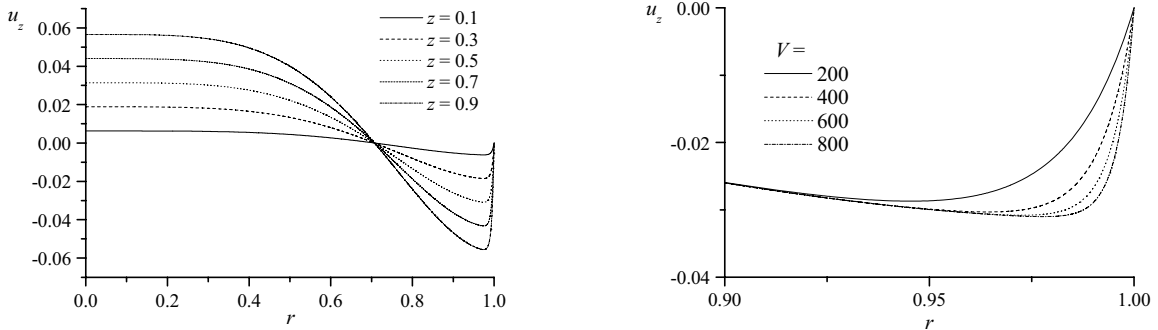


**Figure 10.** We show a) the axial velocity profile at different axial positions; b) the boundary layer profile at increasing vortex Reynolds numbers.

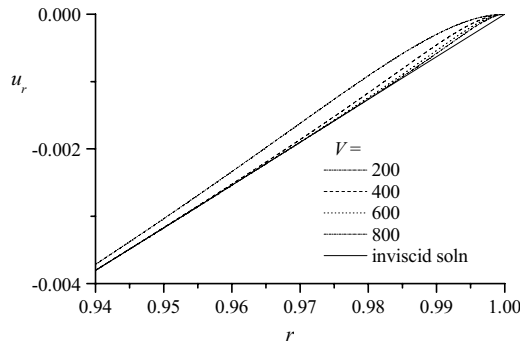


**Figure 11.** We show the radial velocity profile at increasing vortex Reynolds numbers.

## E. Maicke-Majdalani Compressible Vortex (2007)

The purpose of this solution is to achieve an approximation for the bidirectional vortex under compressible, isentropic conditions.

### 1. Motivation

From flows over blunt bodies to airfoil design, the study of compressible motions has almost always been carried out on external flows. The result of this bias is that compressible formulations of many internal flow models are neglected. Recent work attempts to address this discrepancy but there is still much to be realized before our understanding of internal compressible flows becomes as extensive as the work achieved on external flows. There are many reasons for this incongruity. First, many internal flows can be adequately represented by incompressible models. Many flows contained in small spaces do not reach conditions where compressibility effects become a concern. Secondly, compressible formulations of internal flowfields can be difficult to solve analytically for even the most basic representations. When one looks at the more interesting and realistic flowfields, analytical solutions are even harder to come by. As a result, most of the recent work on internal, compressible flows are directed toward numerical studies using either canned or custom CFD packages. While these studies can be useful for specific flows, they do not aid in advancing our understanding of more general flowfields; evidently, their usefulness and predictive capabilities are limited. Finally, the analytical tools that make the solution of these compressible flowfields possible are a relatively recent innovation [44-46]. While perturbation methods have been available for some time, it was not until recently that the methods have been extended to complex engineering problems. Combining perturbation methods with the advent of computer algebra systems leads to insightful solutions previously unreachable.

Since the challenges in acquiring a closed form compressible solution are many, it is important to understand why such solutions are valuable. The first and most fundamental reason is that analytical approximations to these problems enhance our understanding of not only the model being studied, but of fluid dynamics as a whole. Particular solutions often lead to generalized techniques that can be successfully applied to any number of previously abandoned problems. Analytical models are also a helpful supplement to the computational modeling discipline. With the emergence of new and more complicated numerical codes, a fundamental baseline is required to verify their efficacy. Analytical models can provide this baseline, especially in situations where experimental testing of a model is costly or impractical, as is often the case in early rocket motor development. In issues more specific to rocket flow analysis, a compressible model serves as an accurate foundation for stability models, which previously have only considered compressibility in their unsteady components [56-59].

In this paper, we formulate the model for the compressible bidirectional vortex, using a Rayleigh-Janzen perturbation expansion. The solution methodology is outlined and challenges that arise during the solution process are addressed. Some preliminary results are presented and an outline for future work is provided.

### 2. Formulation

In order to extract the compressible analog to the inviscid bidirectional vortex, we employ a Rayleigh-Janzen perturbation in the variables of interest and then expand the governing equations. The result of this technique is that the leading order equations recover the incompressible solution for the flowfield, previously obtained by Vyas and Majdalani [34]. To find the compressible corrections, the first order equations must be solved. These are presented here in the order by which they are considered:

$$\nabla \times (\mathbf{U}^{(0)} \times \boldsymbol{\Omega}^{(1)}) + \nabla \times (\mathbf{U}^{(1)} \times \boldsymbol{\Omega}^{(0)}) = -\frac{\nabla \rho^{(1)} \times \nabla p^{(1)}}{\gamma} \quad (72)$$

$$D^2 \psi^{(1)} + r \boldsymbol{\Omega}^{(1)} = \nabla \rho^{(1)} \cdot \nabla \psi^{(0)} - r \boldsymbol{\Omega}^{(0)} \rho^{(1)} \quad (73)$$

$$-\frac{1}{\gamma} \frac{\partial p^{(2)}}{\partial r} = \rho^{(1)} \left( u_0 \frac{\partial u_r^{(0)}}{\partial r} + u_z^{(0)} \frac{\partial u_r^{(0)}}{\partial z} - \frac{(u_\theta^{(0)})^2}{r} \right) + \frac{\partial (u_r^{(0)} u_r^{(1)})}{\partial r} + u_z^{(0)} \frac{\partial u_r^{(1)}}{\partial z} + u_z^{(1)} \frac{\partial u_r^{(0)}}{\partial z} - 2 \frac{u_\theta^{(0)} u_\theta^{(1)}}{r} \quad (74)$$

$$-\frac{1}{\gamma} \frac{\partial p^{(2)}}{\partial z} = \rho^{(1)} \left( u_z^{(0)} \frac{\partial u_z^{(0)}}{\partial z} + u_r^{(0)} \frac{\partial u_z^{(0)}}{\partial r} \right) + \frac{\partial (u_z^{(0)} u_z^{(1)})}{\partial z} + u_r^{(0)} \frac{\partial u_z^{(1)}}{\partial r} + u_r^{(1)} \frac{\partial u_z^{(0)}}{\partial r} \quad (75)$$

$$\rho^{(2)} = \frac{p^{(2)}}{\gamma} + \frac{1-\gamma}{2\gamma^2} (p^{(1)})^2 \quad (76)$$

$$T^{(2)} = \frac{\gamma-1}{\gamma} p^{(2)} + \frac{1-\gamma}{2\gamma^2} (p^{(1)})^2 \quad (77)$$

$$u_r^{(0)} \left( \frac{\partial u_\theta^{(1)}}{\partial r} + \frac{u_\theta^{(1)}}{r} \right) + u_r^{(1)} \left( \frac{\partial u_\theta^{(0)}}{\partial r} + \frac{u_\theta^{(0)}}{r} \right) = 0 \quad (78)$$

The compressible treatment follows the following strategy. First the vorticity transport equation is used to determine a relationship between the first order vorticity and other previously determined variables. Once this quantity is obtained it is substituted back into the vorticity equation, which allows one to solve for the first order stream function, determining both the radial and axial compressible velocities. The radial and axial momentum equations are then solved to determine the first order pressure correction, followed by substitution into the isentropic relations to fully determine the thermodynamic properties of the flow. The final equation to be solved is the tangential momentum equation, which provides us with the compressible correction to the rotational velocity. At first glance, the solution procedure seems well defined; however there are obstacles that are not readily apparent until the solution is attempted.

### 3. Obstacles

The compressible bidirectional vortex presents a unique set of challenges. In the first iteration of the solution process, we attempt to determine the inviscid, compressible solution to this complex flowfield. Normally, this expansion is straightforward, and can yield a closed form solution with very good accuracy. However, in the bidirectional vortex, there are a number of factors that must be addressed before the Rayleigh-Janzen expansion can be applied.

The first challenge manifests itself in one of the key boundary conditions, namely, the no radial flow across the centerline. This boundary condition is a result of one of the key simplifications, axisymmetry. At the leading order, this boundary condition is satisfied easily via

$$u_r^{(0)}(0, z) = -\frac{1}{r} \frac{\partial \psi^{(0)}}{\partial z} = 0 \quad (79)$$

This equation is easily satisfied and leads to the inviscid stream function solution presented previously. However, for the first order correction in the Mach number squared, the boundary condition is more involved. The equation of interest becomes

$$u_r^{(1)}(0, z) = \frac{\rho^{(1)}}{r} \frac{\partial \psi^{(0)}}{\partial z} - \frac{1}{r} \frac{\partial \psi^{(1)}}{\partial z} = 0 \quad (80)$$

The problem with evaluating this expression stems from the first term on the right-hand-side. The density term, solved after the leading order stream function, is singular at the origin. Because this term is infinite at the origin, this boundary condition cannot be satisfied at the first order, making an accurate compressible correction virtually impossible to achieve. The key is to regularize the problem and include viscosity, at least at the core.

### 4. Weakly viscous approach

To overcome the singularity at the centerline, we use a modified formulation of the inviscid model. Since the majority of the flowfield can be modeled accurately as inviscid, we apply a viscous correction at the core of the flow, where the fluid flow behaves singularly. This viscous core correction eliminates the problem of satisfying the no radial flow across the centerline condition, as well as modifying the tangential momentum equation such that the swirl velocity is no longer incompressible. The result of this is that the tangential momentum equations must be modified. The leading order tangential momentum equation becomes

$$\varepsilon \frac{d^2 \xi^{(0)}}{d\eta^2} - \frac{u_r^{(0)}}{2\sqrt{\pi\eta}} \frac{d\xi^{(0)}}{d\eta} = 0 \quad (81)$$

Similarly, the first order representation yields

$$\varepsilon \frac{d^2 \xi^{(1)}}{d\eta^2} - \frac{u_r^{(0)}}{2\sqrt{\pi\eta}} \frac{d\xi^{(1)}}{d\eta} - \frac{u_r^{(1)}}{2\sqrt{\pi\eta}} \frac{d\xi^{(0)}}{d\eta} - \frac{\rho^{(1)} u_r^{(0)}}{2\sqrt{\pi\eta}} \frac{d\xi^{(0)}}{d\eta} = 0 \quad (82)$$

As before, we take  $\xi = ru_\theta$ ,  $\eta = \pi r^2$ , and  $\varepsilon = 1/Re$ . Unsurprisingly the leading order equation recovers the incompressible solution of Vyas and Majdalani [60]. This solution is determined by first suppressing the viscous term to find the outer solution, and then introducing an inner scale to capture the viscous behavior near the core.

Because the viscosity change only modifies the tangential momentum equation, the solution methodology outlined previously will still apply. The only change to the procedure is that the composite solution is utilized in lieu of the free vortex.

Armed with this new composite swirl velocity, we can now return to and solve Eqs. (72)-(77) for the first order corrections. The substitution of this swirl velocity with the core correction enables us to revisit Eq. (73) in particular. Because of the viscous core correction, the density is no longer singular at the origin; the previously troublesome boundary condition, Eq. (80) can now be successfully applied to find the compressible stream function correction. The full first order stream function is a cumbersome expression. However, consistent with perturbation methods, there are some terms in the relation that are smaller than the order of accuracy of the expansion. These terms may be truncated, and the remaining expression will still capture the behavior of the first order correction. The resulting expression is

$$\psi^{(1)} = \begin{cases} \frac{\pi^2 B^3 z^3}{3} \sin(\pi r^2) \left[ 6 + \cos(2\pi r^2) - \cos(2\pi \beta^2) \right] + \frac{Bz}{8} e^{-r^2 V/2} \left[ (2e^{r^2 V/4} - 1) 4\pi \cos \pi r^2 \right. \\ \left. + e^{r^2 V/2} \left\{ \pi \cos \pi r^2 \left[ -2(2 + r^2 V) \text{Ei}\left(-\frac{r^2 V}{2}\right) + 2(4 + r^2 V) \text{Ei}\left(-\frac{r^2 V}{4}\right) - 2(4 + 9B^2) \ln r + (r^2 - 1)\phi \right] \right. \right. \\ \left. \left. + (\chi - \lambda) \sin \pi r^2 \right] \right\} \end{cases} \quad (83)$$

where  $B = Q_i \csc(\pi \beta^2) / (2\pi l)$ ,  $\beta$  is the outlet radius,  $\mathcal{E}$  is the Euler gamma constant,  $V = \bar{Q}_i / L\nu$ ,

$$\phi = 4 + 4\mathcal{E} - 12 \ln 2 + B^2 \ln 1024\pi^9 + 4 \ln V \quad (84)$$

$$\lambda = \pi \csc \pi \beta^2 \left\{ \begin{aligned} & 4\text{Ci}(\pi \beta^2) + \ln \frac{1}{4096\pi^4} + \cos \pi \beta^2 \left[ \ln 4096 + 4(\beta^2 - 1) \ln V \right] \\ & - 2 \ln(V^2 + 4\pi^2) + 4 \ln(V^2 + 16\pi^2) + 9B^2 \sin \pi \beta^2 \text{Si}(2\pi \beta^2) \end{aligned} \right\} \quad (85)$$

and

$$\chi = 2V \left( \tan^{-1} \frac{2\pi}{V} - \tan^{-1} \frac{4\pi}{V} \right) \csc \pi \beta^2 \quad (86)$$

All of which are constants for a given chamber. While this solution is relatively compact in the simplified form, it is difficult to carry all of the information forward. The compressible stream function only determines the compressible axial and radial velocities. Knowledge of these terms is required to solve Eq. (82), which determines the swirl velocity. It is possible to use the full expression for the stream function to determine the swirl velocity, but the resulting solution contains an integral formulation. There are a number of other methods that can be employed to achieve a solution. The first method is to neglect the  $u_r^{(1)}$  velocity term in Eq. (82). Since the swirl velocity dominates the compressible terms, neglecting this term results in a compact equation that provides an approximate solution for the compressible swirl velocity. The second method is to employ a further reduced stream function, carrying forward only the most dominant terms. This method offers a slightly more accurate expression for the swirl velocity, albeit at the cost of increased complexity.

There are a number of additional challenges that have yet to be met. A more comprehensive model for the bidirectional vortex is our goal. Uniting the work done in determining the viscous boundary layers along the walls and corners of the chamber to the compressible solution will provide an even more accurate platform for stability prediction and analysis. The relaxation of the limiting assumptions also constitutes a vital area of interest for further studies. Finding a vortex model that is not dependent on the isentropic flow condition is an intriguing area that must be undertaken in the process of paving the way for a successful thermal analysis of the combustion chamber. A solution that does not neglect the axial variations of the swirl velocity is also of particular interest. Having an analytical comparison between the original solution and the one with axial variations would be very helpful.

### Acknowledgments

The authors are grateful for the support received from ORBITEC (FA8650-05-C-2612) and from the National Science Foundation (CMS-0353518). The authors acknowledge useful discussions with Martin J. Chiaverini of Orbital Technologies Corporation (ORBITEC), Madison, WI.

## References

- [1] Penner, S. S., "Elementary Considerations of the Fluid Mechanics of Tornadoes and Hurricanes," *Acta Astronautica*, Vol. 17, 1972, pp. 351-362.
- [2] Königl, A., "Stellar and Galactic Jets: Theoretical Issues," *Canadian Journal of Physics*, Vol. 64, 1986, pp. 362-368.
- [3] Kirshner, R. P., *The Extravagant Universe: Exploding Stars, Dark Energy, and the Accelerating Cosmos*, Princeton University Press, Princeton, New Jersey, 2004.
- [4] Reydon, R. F., and Gauvin, W. H., "Theoretical and Experimental Studies of Confined Vortex Flow," *The Canadian Journal of Chemical Engineering*, Vol. 59, 1981, pp. 14-23.
- [5] Chiaverini, M. J., Malecki, M. J., Sauer, J. A., Knuth, W. H., and Majdalani, J., "Vortex Thrust Chamber Testing and Analysis for O<sub>2</sub>-H<sub>2</sub> Propulsion Applications," AIAA Paper 2003-4473, July 2003.
- [6] Chiaverini, M. J., Malecki, M. M., Sauer, J. A., Knuth, W. H., and Hall, C. D., "Testing and Evaluation of Vortex Combustion Chamber for Liquid Rocket Engines," JANNAF 2002.
- [7] Chiaverini, M. J., Malecki, M. J., Sauer, J. A., and Knuth, W. H., "Vortex Combustion Chamber Development for Future Liquid Rocket Engine Applications," AIAA Paper 2002-2149, July 2002.
- [8] Vyas, A. B., Majdalani, J., and Chiaverini, M. J., "The Bidirectional Vortex. Part 3: Multiple Solutions," AIAA Paper 2003-5054, July 2003.
- [9] Harvey, J. K., "Some Observations of the Vortex Breakdown Phenomenon," *Journal of Fluid Mechanics*, Vol. 14, No. 4, 1962, pp. 585-592.
- [10] Sarpkaya, T., "On Stationary and Travelling Vortex Breakdowns," *Journal of Fluid Mechanics*, Vol. 45, No. 3, 1971, pp. 545-559.
- [11] Leibovich, S., "The Structure of Vortex Breakdown," *Annual Review of Fluid Mechanics*, Vol. 10, 1978, pp. 221-246.
- [12] Leibovich, S., "Vortex Stability and Breakdown: Survey and Extension," *AIAA Journal*, Vol. 22, No. 9, 1984, pp. 1192-1206.
- [13] Lilley, D. G., "Swirl Flows in Combustion: A Review," *AIAA Journal*, Vol. 15, No. 8, 1977, pp. 1063-1078.
- [14] Gupta, A. K., Lilley, D. G., and Syred, N., *Swirl Flows*, Abacus, London, UK, 1984.
- [15] Durbin, M. D., Vangsness, M. D., Ballal, D. R., and Katta, V. R., "Study of Flame Stability in a Step-Swirl Combustor," *Journal of Engineering for Gas Turbines and Power-Transactions of the ASME*, Vol. 118, 1996, pp. 308-314.
- [16] Lewellen, W. S., "A Review of Confined Vortex Flows," NASA, Technical Rept. CR-1772, July 1971.
- [17] Vatisistas, G. H., Lin, S., and Kwok, C. K., "Theoretical and Experimental Studies on Vortex Chamber Flows," *AIAA Journal*, Vol. 24, No. 4, 1986, pp. 635-642.
- [18] Vatisistas, G. H., Lin, S., and Kwok, C. K., "Reverse Flow Radius in Vortex Chambers," *AIAA Journal*, Vol. 24, No. 11, 1986, pp. 1872-1873.
- [19] Vatisistas, G. H., Jawarneh, A. M., and Hong, H., "Flow Characteristics in a Vortex Chamber," *The Canadian Journal of Chemical Engineering*, Vol. 83, No. 6, 2005, pp. 425-436.
- [20] Flinn, E. D., "Cooling of a Hot New Engine," in *Aerospace America* 2001, Vol. 39, pp. 26-27.
- [21] Rankine, W. J. M., *A Manual of Applied Mechanics*, 9th ed., C. Griffin and Co., London, UK, 1858.
- [22] Mallen, K. J., Montgomery, M. T., and Wang, B., "Reexamining the near-Core Radial Structure of the Tropical Cyclone Primary Circulation: Implications for Vortex Resiliency," *Journal of the Atmospheric Sciences*, Vol. 62, No. 2, 2005, pp. 408-425.
- [23] Wendt, B. J., "Initial Circulation and Peak Vorticity Behavior of Vortices Shed from Airfoil Vortex Generators," NASA, Technical Rept. NASA/CR—2001-211144, August 2001.
- [24] Alekseenko, S. V., Kuibin, P. A., Okulov, V. L., and Shtork, S. I., "Helical Vortices in Swirl Flow," *Journal of Fluid Mechanics*, Vol. 382, No. 1, 1999, pp. 195-243.
- [25] Schmid, P. J., and Rossi, M., "Three-Dimensional Stability of a Burgers Vortex," *Journal of Fluid Mechanics*, Vol. 500, No. 1, 2004, pp. 103-112.
- [26] Pérez-Saborid, M., Herrada, M. A., Gómez-Barea, A., and Barrero, A., "Downstream Evolution of Unconfined Vortices: Mechanical and Thermal Aspects," *Journal of Fluid Mechanics*, Vol. 471, No. 1, 2002, pp. 51-70.

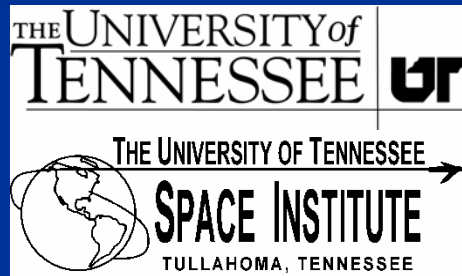
- [27] Eloy, C., and Le Dizès, S., "Three-Dimensional Instability of Burgers and Lamb-Oseen Vortices in a Strain Field," *Journal of Fluid Mechanics*, Vol. 378, No. 1, 1999, pp. 145-166.
- [28] Devenport, W. J., Rife, M. C., Liapis, S. I., and Follin, G. J., "The Structure and Development of a Wing-Tip Vortex," *Journal of Fluid Mechanics*, Vol. 312, No. 1, 1996, pp. 67-106.
- [29] Faler, J. H., and Leibovich, S., "Disrupted States of Vortex Flow and Vortex Breakdown," *Physics of Fluids*, Vol. 20, No. 9, 1977, pp. 1385-1400.
- [30] Escudier, M. P., "Vortex Breakdown - Observations and Explanations," *Progress in Aerospace Sciences*, Vol. 25, No. 2, 1988, pp. 189-229.
- [31] Long, R. R., "A Vortex in an Infinite Viscous Fluid," *Journal of Fluid Mechanics*, Vol. 11, No. 4, 1961, pp. 611-624.
- [32] Sullivan, R. D., "A Two-Cell Vortex Solution of the Navier-Stokes Equations," *Journal of the Aerospace Sciences*, Vol. 26, 1959, pp. 767-768.
- [33] Bloor, M. I. G., and Ingham, D. B., "The Flow in Industrial Cyclones," *Journal of Fluid Mechanics*, Vol. 178, No. 1, 1987, pp. 507-519.
- [34] Vyas, A. B., and Majdalani, J., "Exact Solution of the Bidirectional Vortex," *AIAA Journal*, Vol. 44, No. 10, 2006, pp. 2208-2216.
- [35] Bloor, M. I. G., and Ingham, D. B., "Theoretical Investigation of the Flow in a Conical Hydrocyclone," *Transactions of the Institution of Chemical Engineers*, Vol. 51, No. 1, 1973, pp. 36-41.
- [36] Kelsall, D. F., "A Study of Motion of Solid Particles in a Hydraulic Cyclone," *Transactions of the Institution of Chemical Engineers*, Vol. 30, 1952, pp. 87-103.
- [37] Vyas, A. B., Majdalani, J., and Chiaverini, M. J., "The Bidirectional Vortex. Part 1: An Exact Inviscid Solution," AIAA Paper 2003-5052, July 2003.
- [38] Majdalani, J., and Rienstra, S. W., "On the Bidirectional Vortex and Other Similarity Solutions in Spherical Coordinates," *Journal of Applied Mathematics and Physics (ZAMP)*, Vol. 58, No. 1, 2007.
- [39] Vyas, A. B., Majdalani, J., and Chiaverini, M. J., "The Bidirectional Vortex. Part 2: Viscous Core Corrections," AIAA Paper 2003-5053, July 2003.
- [40] Anderson, M. H., Valenzuela, R., Rom, C. J., Bonazza, R., and Chiaverini, M. J., "Vortex Chamber Flow Field Characterization for Gelled Propellant Combustor Applications," AIAA Paper 2003-4474, July 2003.
- [41] Vyas, A. B., and Majdalani, J., "Characterization of the Tangential Boundary Layers in the Bidirectional Vortex Thrust Chamber," AIAA Paper 2006-4888, July 2006.
- [42] Batterson, J. W., and Majdalani, J., "On the Boundary Layers of the Bidirectional Vortex " AIAA Paper 2007-4123 June 2007.
- [43] Maicke, B. A., and Majdalani, J., "The Compressible Bidirectional Vortex " AIAA Paper 2007-4122, June 2007.
- [44] Majdalani, J., "On Steady Rotational High Speed Flows: The Compressible Taylor-Culick Profile," *Proceedings of the Royal Society, Series A*, Vol. 463, No. 2077, 2007, pp. 131-162.
- [45] Majdalani, J., "The Compressible Taylor-Culick Flow," AIAA Paper 2005-3542, July 2005.
- [46] Maicke, B. A., and Majdalani, J., "The Compressible Taylor Flow in Slab Rocket Motors," AIAA Paper 2006-4957, July 2006.
- [47] Smith, J. L., "An Analysis of the Vortex Flow in the Cyclone Separator," *Journal of Basic Engineering-Transactions of the ASME*, 1962, pp. 609-618.
- [48] Hoekstra, A. J., Derksen, J. J., and Van den Akker, H. E. A., "An Experimental and Numerical Study of Turbulent Swirling Flow in Gas Cyclones," *Chemical Engineering Science*, Vol. 54, No. 13, 1999, pp. 2055-2065.
- [49] Balachandar, S., Buckmaster, J. D., and Short, M., "The Generation of Axial Vorticity in Solid-Propellant Rocket-Motor Flows," *Journal of Fluid Mechanics*, Vol. 429, No. 1, 2001, pp. 283-305.
- [50] Murray, A. L., Gudgen, A. J., Chiaverini, M. J., Sauer, J. A., and Knuth, W. H., "Numerical Code Development for Simulating Gel Propellant Combustion Processes," 52nd JANNAF Paper (Technical), May 2004.
- [51] Rom, C. J., Anderson, M. H., and Chiaverini, M. J., "Cold Flow Analysis of a Vortex Chamber Engine for Gelled Propellant Combustor Applications," AIAA Paper 2004-3359, July 2004.
- [52] Hu, L. Y., Zhou, L. X., Zhang, J., and Shi, M. X., "Studies of Strongly Swirling Flows in the Full Space of a Volute Cyclone Separator," *AIChE Journal*, Vol. 51, No. 3, 2005, pp. 740-749.
- [53] Prandtl, L., "Zur Berechnung Der Grenzschichten," *ZAMM*, No. 18, 1938, pp. 77-82.

- [54] Conlisk, A. T., "Source-Sink Flows in a Rapidly Rotating Annulus," Dissertation, Purdue, 1978.
- [55] Vyas, A. B., Majdalani, J., and Chiaverini, M. J., "Characterization of the Tangential Boundary Layers in the Bidirectional Vortex Thrust Chamber," AIAA Paper 2006-8888, 9-12 July 2006.
- [56] Majdalani, J., "The Boundary Layer Structure in Cylindrical Rocket Motors," *AIAA Journal*, Vol. 37, No. 4, 1999, pp. 505-508.
- [57] Majdalani, J., and Flandro, G. A., "The Oscillatory Pipe Flow with Arbitrary Wall Injection," *Proceedings of the Royal Society, Series A*, Vol. 458, No. 2022, 2002, pp. 1621-1651.
- [58] Majdalani, J., Flandro, G. A., and Roh, T. S., "Convergence of Two Flowfield Models Predicting a Destabilizing Agent in Rocket Combustion," *Journal of Propulsion and Power*, Vol. 16, No. 3, 2000, pp. 492-497.
- [59] Majdalani, J., and Van Moorhem, W. K., "Improved Time-Dependent Flowfield Solution for Solid Rocket Motors," *AIAA Journal*, Vol. 36, No. 2, 1998, pp. 241-248.
- [60] Vyas, A. B., and Majdalani, J., "Characterization of the Tangential Boundary Layers in the Bidirectional Vortex Thrust Chamber," AIAA Joint Propulsion Conference Paper 2006-4888, 2006.

# Advancements in Theoretical Models of Confined Vortex Flowfields

by

Joshua W. Batterson, Brian A. Maicke and Joe Majdalani



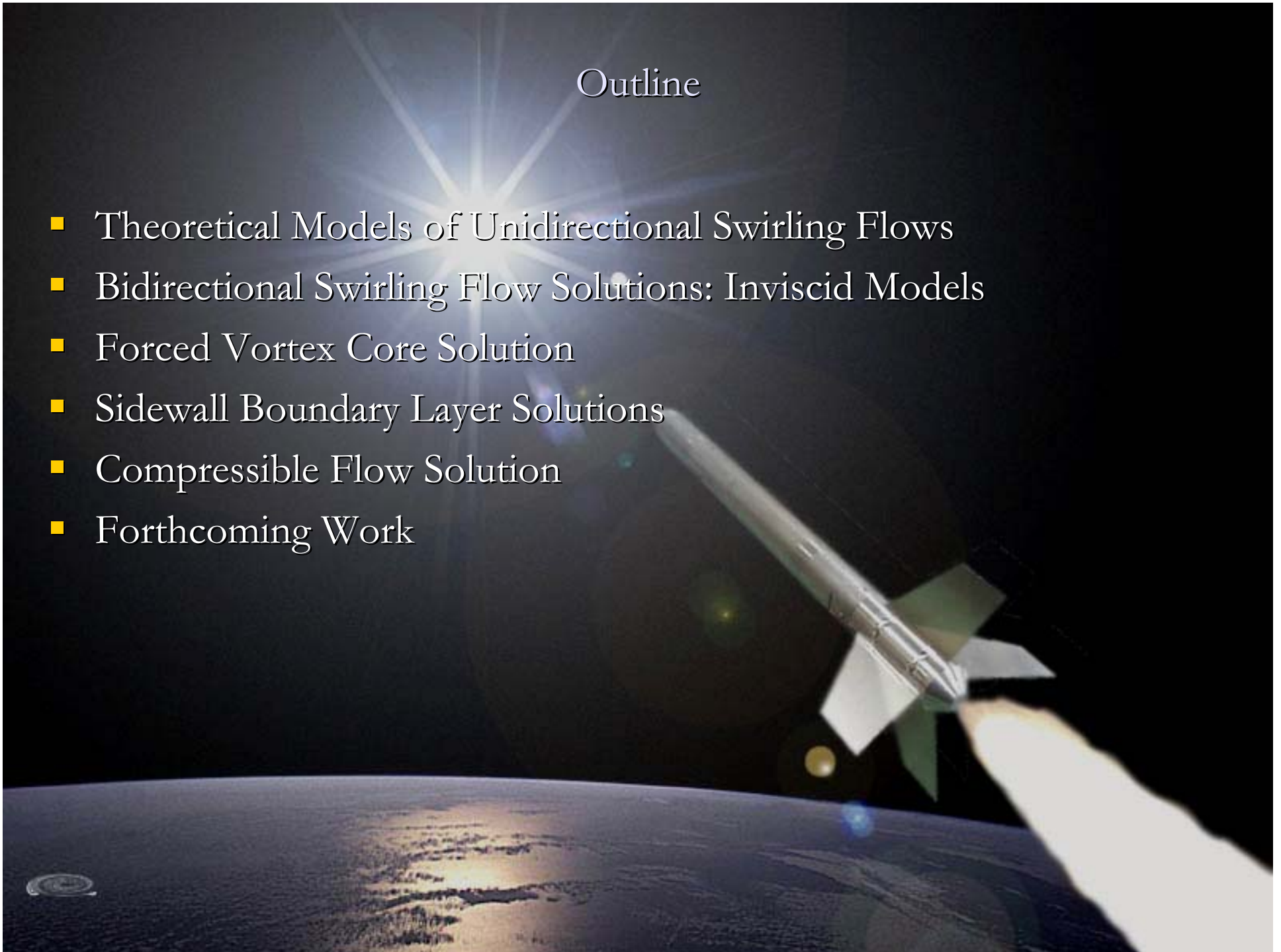
Prepared for  
**2007 JANNAF Propulsion Meeting**  
**Liquid Rocket Engine Chamber Development**

May 14-17, 2007  
Denver, CO

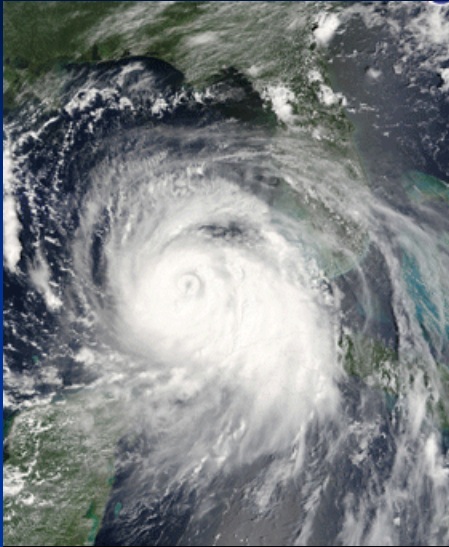


## Outline

- Theoretical Models of Unidirectional Swirling Flows
- Bidirectional Swirling Flow Solutions: Inviscid Models
- Forced Vortex Core Solution
- Sidewall Boundary Layer Solutions
- Compressible Flow Solution
- Forthcoming Work



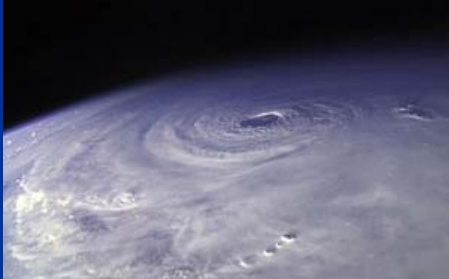
# Natural Phenomena



Galactic pinwheels



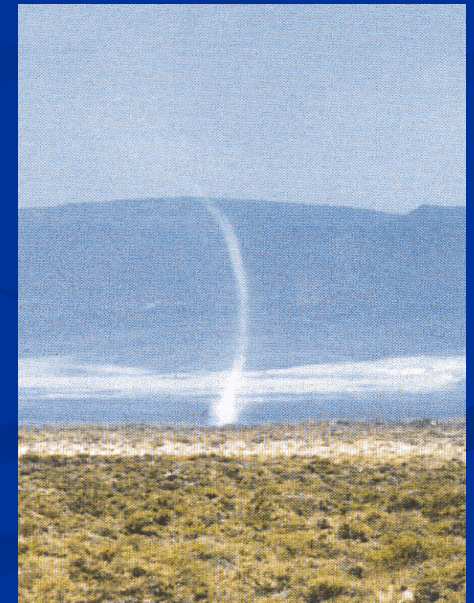
Waterspouts



Hurricanes/typhoons:  
tropical cyclones



Tornados

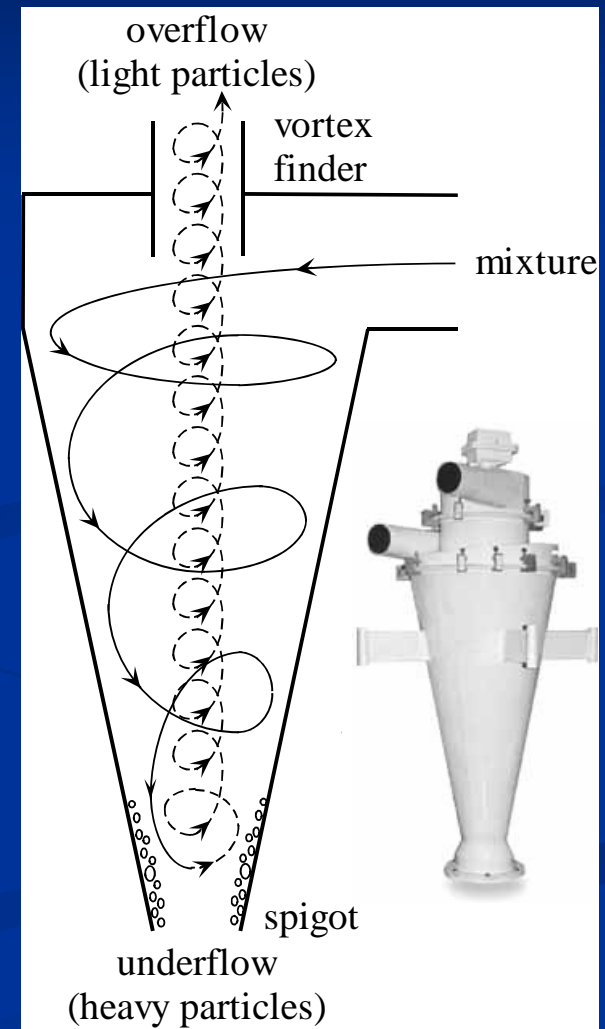
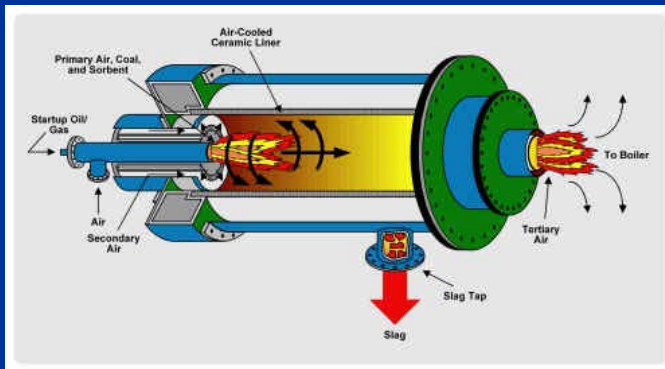


Dust devils

Vortex	Equation	Graphical Representation
Rankine (1858)	$u_{\theta}(r) = \begin{cases} \frac{u_{\max} r}{\delta_c}, & r < \delta_c \\ \frac{u_{\max} \delta_c}{r}, & r \geq \delta_c \end{cases}$	<p>Rankine combined vortex (1858)</p>
Lamb-Oseen (1932)	$u_{\theta}(r) = \frac{\Gamma}{2\pi r} \left[ 1 - \exp\left(-\frac{1}{4\nu t} r^2\right) \right]$	<p>Oseen-Lamb vortex (1932)</p>
Burgers-Rott (1948)	$u_{\theta}(r) = \frac{\Gamma}{2\pi r} \left[ 1 - \exp\left(-\frac{\alpha}{2\nu} r^2\right) \right]$	<p>Burgers-Rott vortex (1948)</p>
Sullivan's Two-Cell Vortex (1959)	$u_{\theta}(r) = \frac{\Gamma}{2\pi r} \frac{1}{H(\infty)} H\left(\frac{\alpha}{2\nu} r^2\right)$ $H(x) = \int_0^x e^{f(t)} dt$ $f(t) = -t + 3 \int_0^t (1 - e^{-y}) \frac{dy}{y}$	<p>Sullivan vortex (1959)</p>

## Uses in Industry: Cyclonic Separators and Furnaces

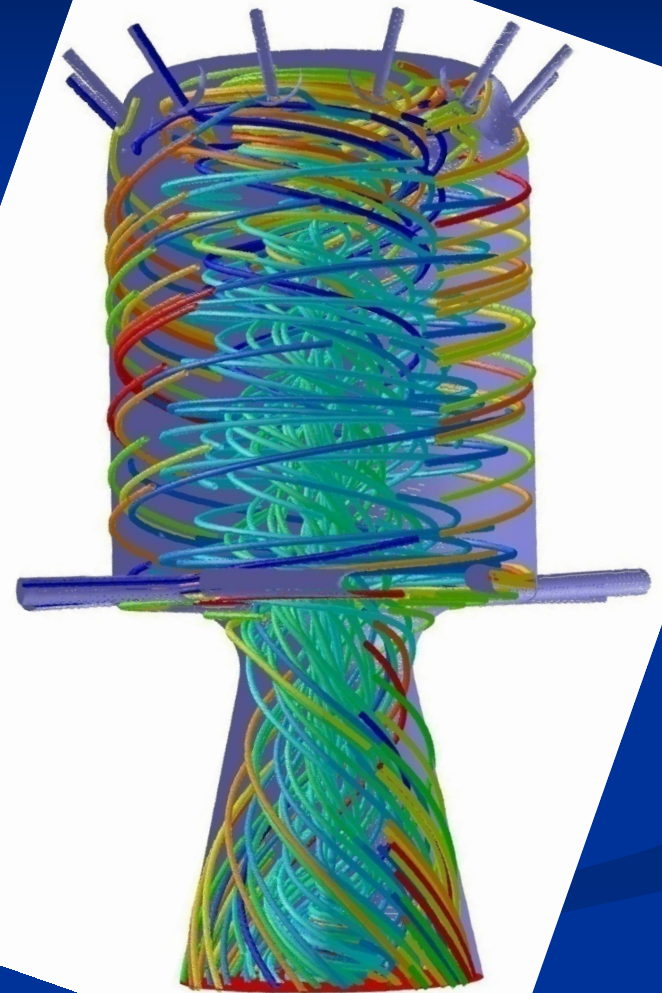
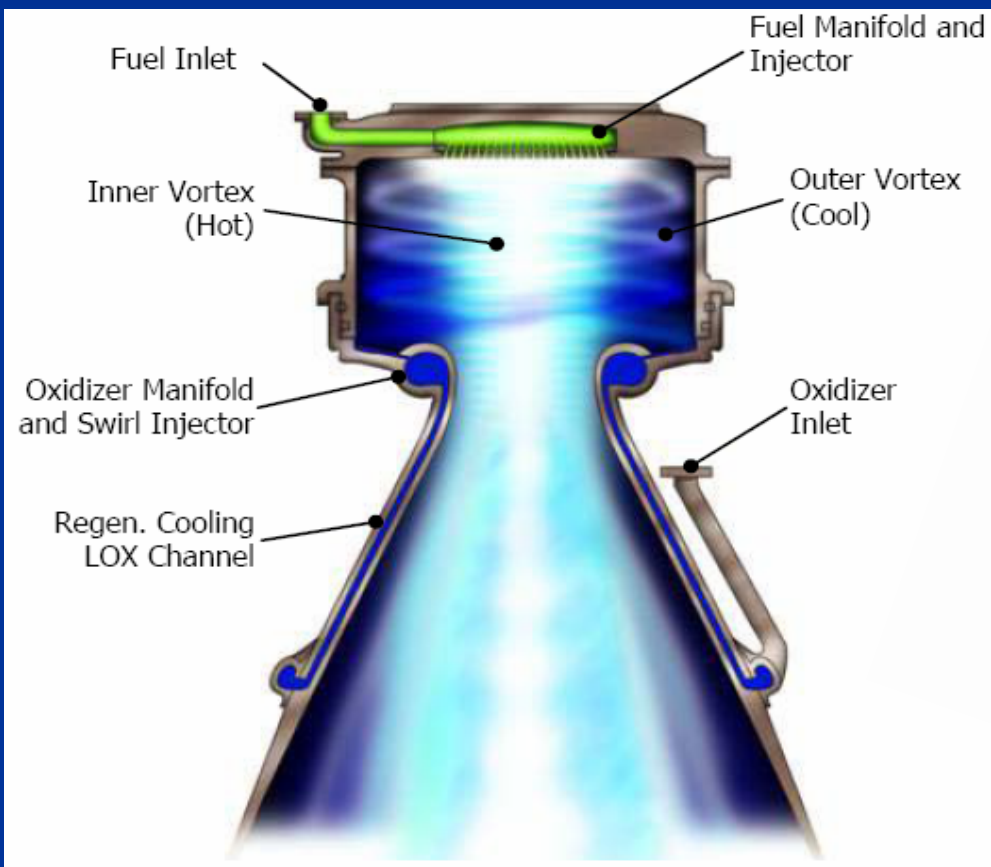
- ter Linden: Exp, Delft U. of Technology, 1949
- Kelsall: Exp, AERE, 1952
- Smith: Exp-Theo, MIT, 1962
- Bloor & Ingham: Theo, Univ. of Leeds, 1987
- Hsieh & Rajamani: Exp-Num, UoU, 1991
- Hoekstra, Derksen & Van den Akker: Exp-Num, Delft Univ. of Technology, 2000
- Hu *et al.*: Exp-Num, Tsinghua Univ., 2005





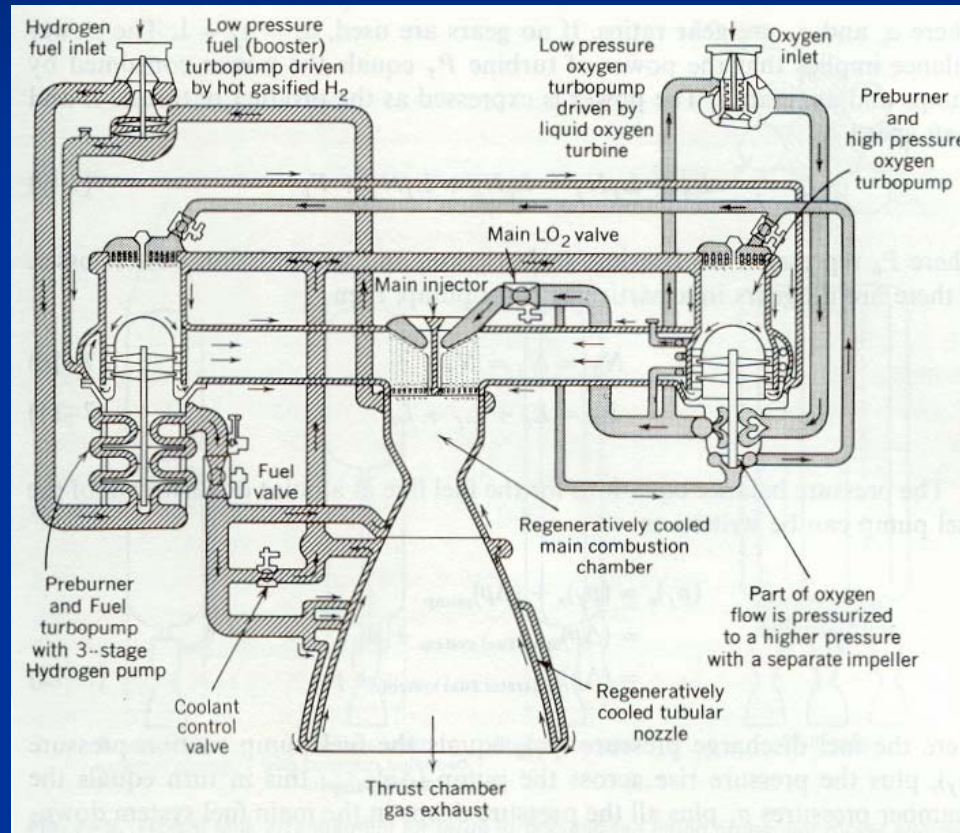
# Propulsive Application – ORBITEC Vortex Engine

- Swirl and injection-driven flows

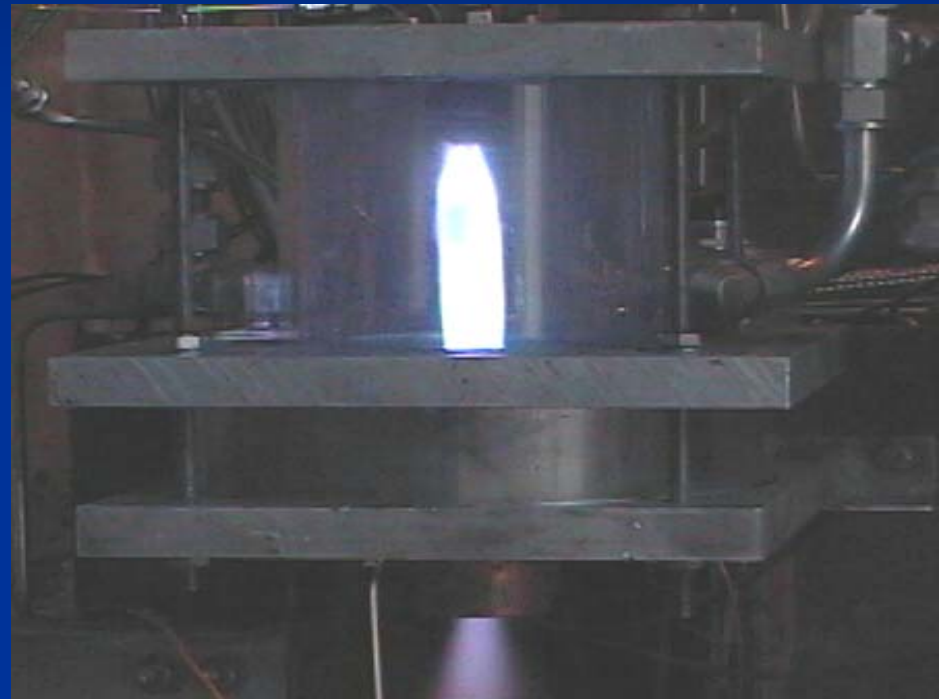


# Conventional Liquid Propellant Thrust Engines

## V-2 Rocket (1944)–SSME (1990)

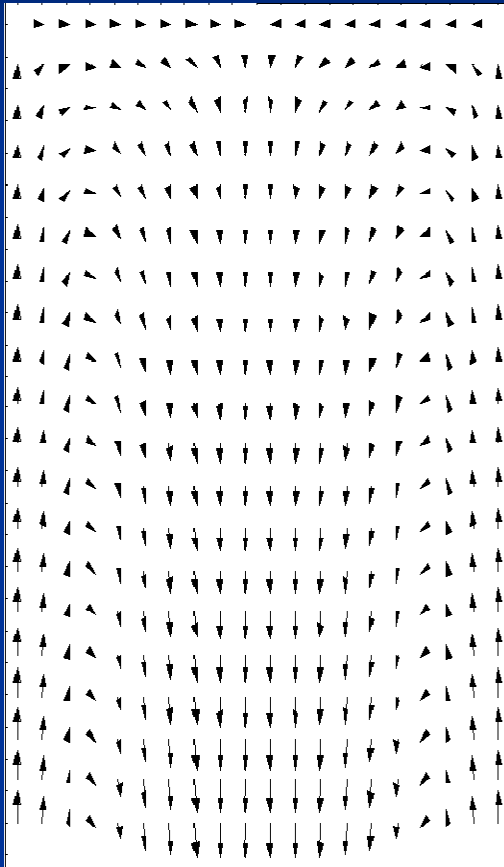


# Laboratory Demonstration

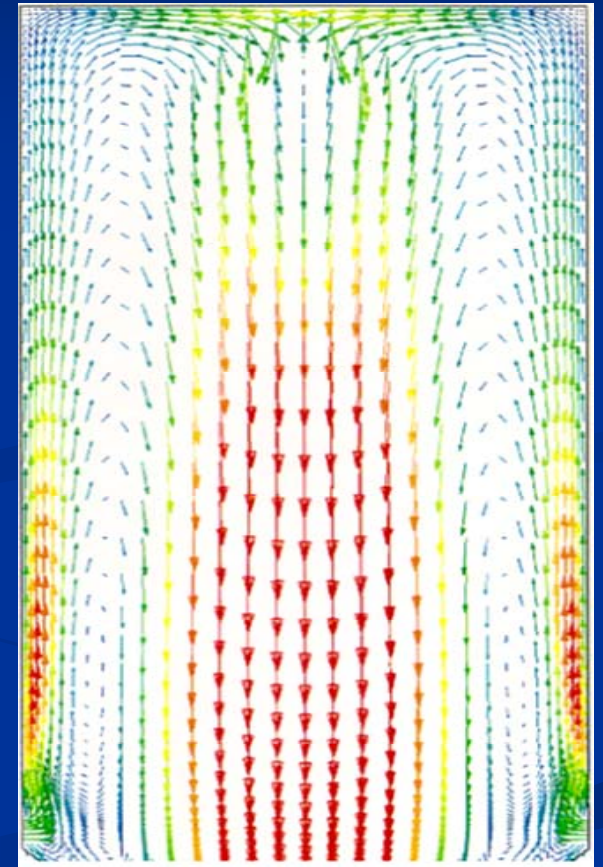




## Analytical vs. Numerical Vector Fields



$$\begin{cases} U_r = -\frac{\kappa}{r} \sin(\pi r^2) \left[ 1 - e^{-\frac{1}{4}\alpha(1-r^2)V} \right] \\ U_\theta = \frac{1}{r} \left[ 1 - e^{-\frac{1}{4}Vr^2} - e^{-\frac{1}{4}\alpha(1-r^2)V} \right] \\ U_z = 2\pi\kappa z \cos(\pi r^2) \left[ 1 - e^{-\frac{1}{4}\alpha(1-r^2)V} \right] \end{cases}$$
$$\alpha = \left( \frac{1}{6}\pi^2 - 1 \right); V = \frac{\text{Re } a}{\sigma L}$$





# Supporting Studies of Bidirectional Vortex Models

Vyas, Majdalani and Chiaverini, "The Bidirectional Vortex. Part 1: An Exact Inviscid Solution," AIAA Paper 2003-5052, July 2003. Now in AIAA Journal 2006.

Vyas, Majdalani and Chiaverini, "The Bidirectional Vortex. Part 2: Viscous Core Corrections," AIAA Paper 2003-5053, July 2003.

Vyas, Majdalani and Chiaverini, "The Bidirectional Vortex. Part 3: Multiple Solutions," AIAA Paper 2003-5054, July 2003.

Majdalani and Rienstra, "On the Bidirectional Vortex and Other Similarity Solutions in Spherical Geometry," AIAA Paper 2004-3675, July 2004. Now in ZAMP.

Sams and Majdalani, "The Conical Bidirectional Vortex," AIAA Paper 2005-4532, July 2005.

Majdalani and Vyas, "Rotational Axisymmetric Mean Flow for the Vortex Injection Hybrid Rocket Engine," AIAA Paper 2004-3475, July 2004. Now in AIAA Progress Series.

Fang, Majdalani and Chiaverini, "Simulation of the Cold-Wall Swirl Driven Combustion Chamber," AIAA Paper 2003-5055, July 2003.

Fang, Majdalani and Chiaverini, "Hot Flow Model of the Vortex Cold Wall Liquid Rocket," AIAA Paper 2004-3676, July 2004.

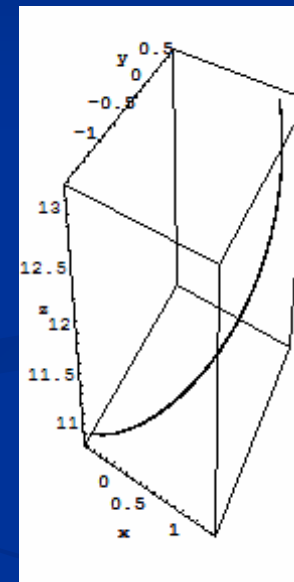
Abu-Irshaid, Majdalani and Casalis, "Hydrodynamic Instability of the Bidirectional Vortex," AIAA Paper 2005-4531, July 2005.

Vyas and Majdalani, "Characterization of the Tangential Boundary Layers in the Bidirectional Vortex Thrust Chamber," AIAA Paper 2006-4888, July 2006. Soon in AIAA Journal.

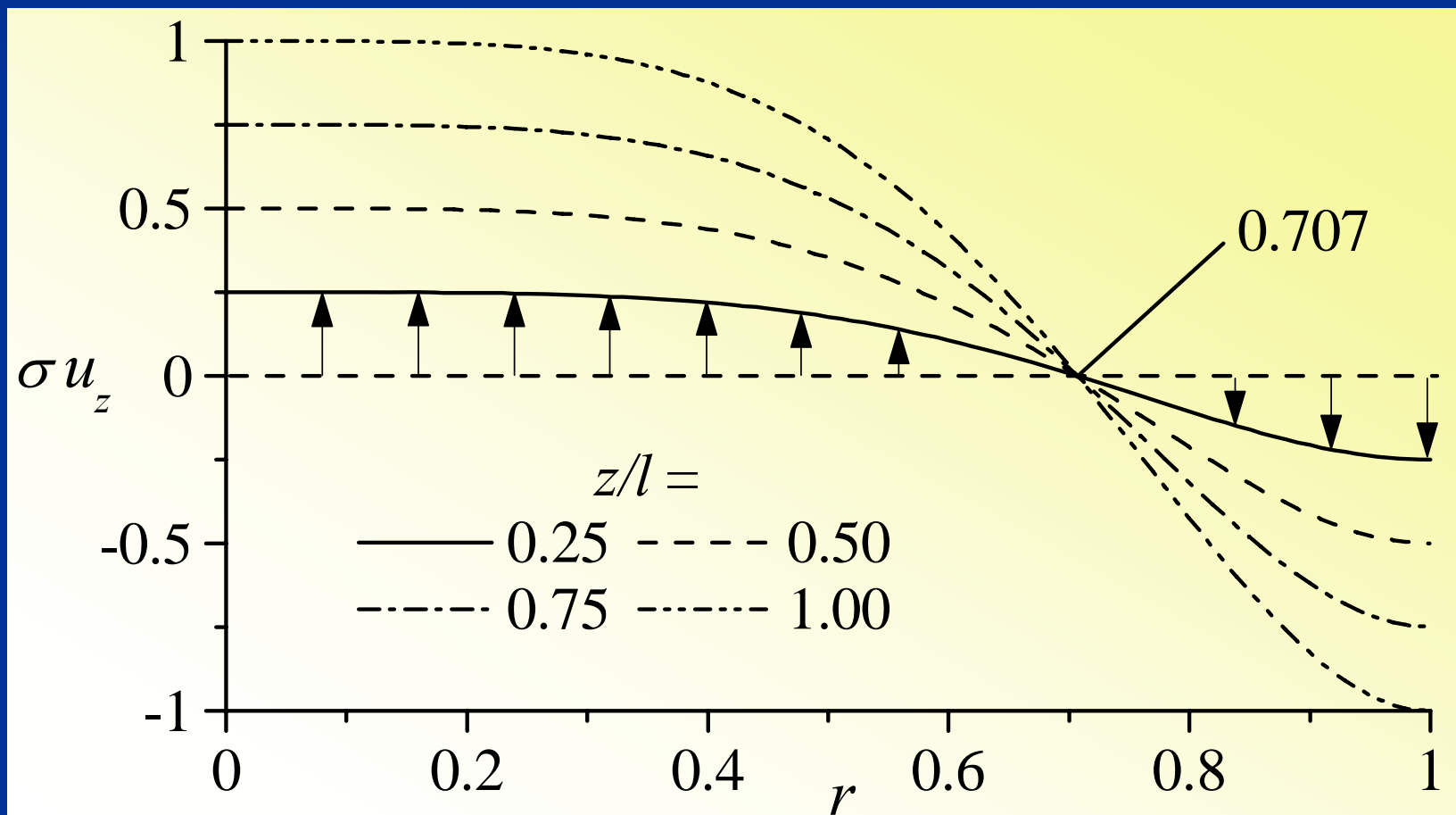
## Animated Analytical Solution (Exact Inviscid)

$$\begin{cases} u_r = -\frac{\kappa}{r} \sin(\pi r^2) \\ u_\theta = \frac{1}{r} \\ u_z = 2\pi\kappa z \cos(\pi r^2) \end{cases}$$

$$\kappa \equiv \frac{A_i}{2\pi a L} = \frac{1}{2\pi \sigma l}$$

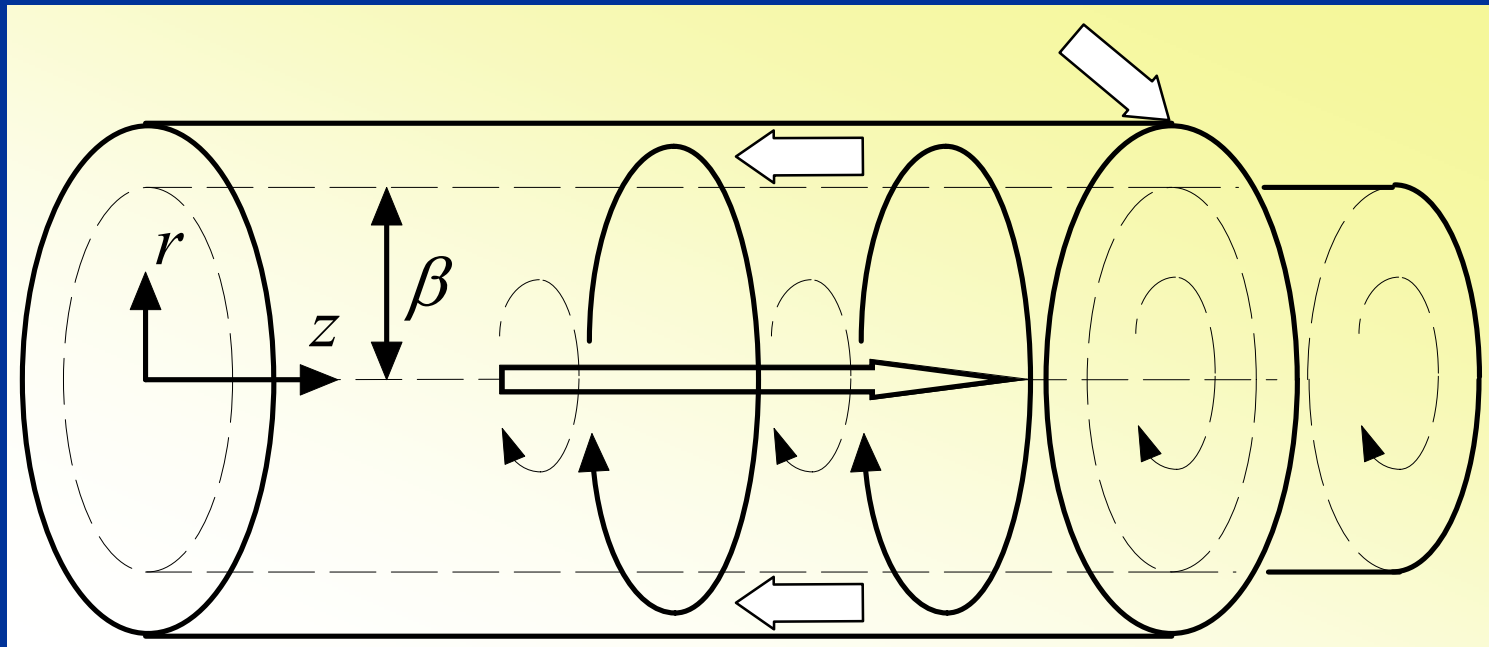


$$\mathbf{u} = -\frac{\sin(\pi r^2)}{2\pi\sigma l \sin(\pi\beta^2)r} \mathbf{e}_r + \frac{1}{r} \mathbf{e}_\theta + \frac{z}{\sigma l \sin(\pi\beta^2)} \cos(\pi r^2) \mathbf{e}_z$$



## Locus of the Mantle (AIAA 2003-5052)

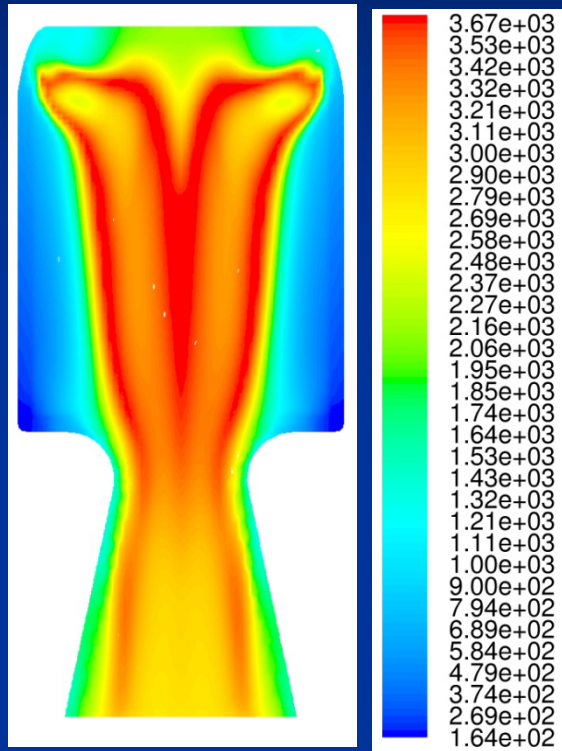
$$\cos(\pi\beta^2) = 0 \quad \therefore \quad \beta = \frac{1}{\sqrt{2}} \cong 0.707$$



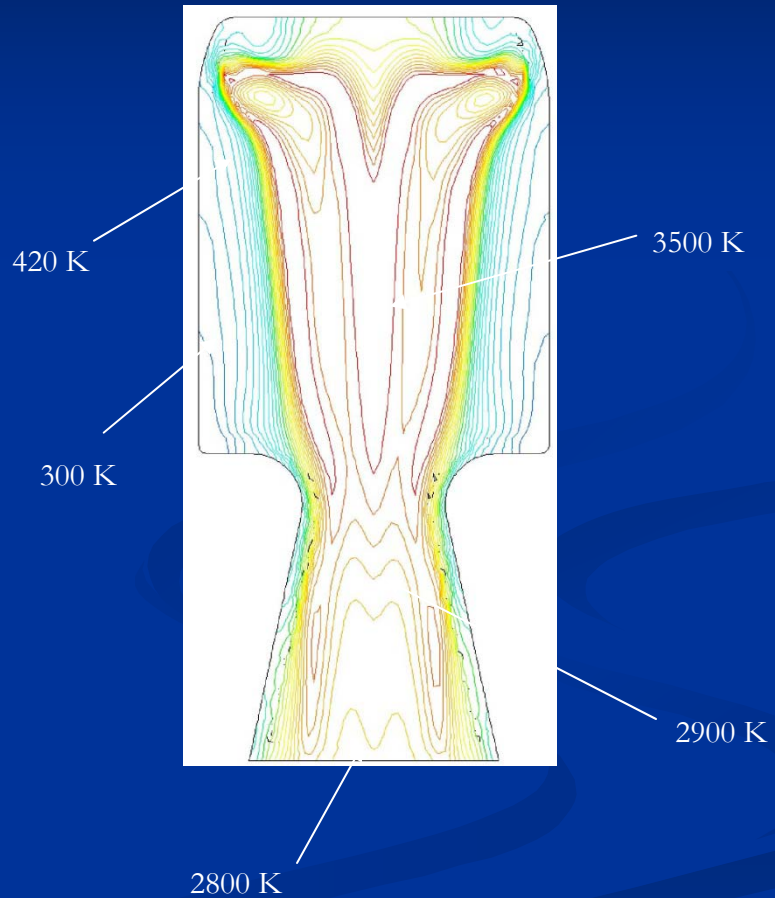
## Experimental Confirmation by J. L. Smith (MIT)

Site	$L - \bar{z}$ [in]	$\bar{r}$ [in]	Radial Fraction, $\beta^*$
1	0.0	2.13	0.7083
2	1.5	2.15	0.7166
3	3.0	2.15	0.7166
4	4.5	2.15	0.7166
5	6.0	2.17	0.7233
6	7.5	2.20	0.7333
7	9.0	2.20	0.7333
Mean		2.16	0.7211

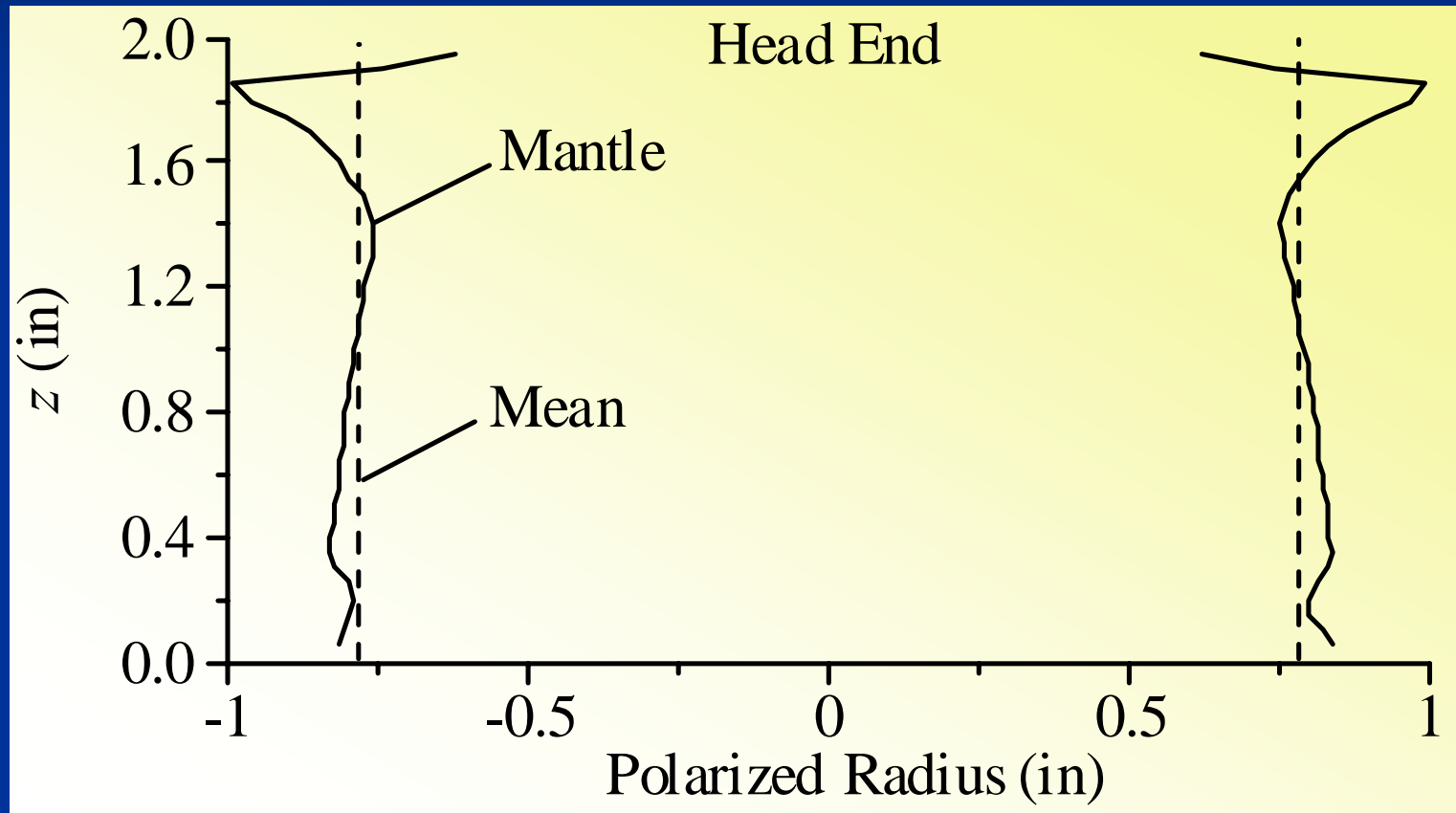
# Isotherms Under Reactive Flow Conditions



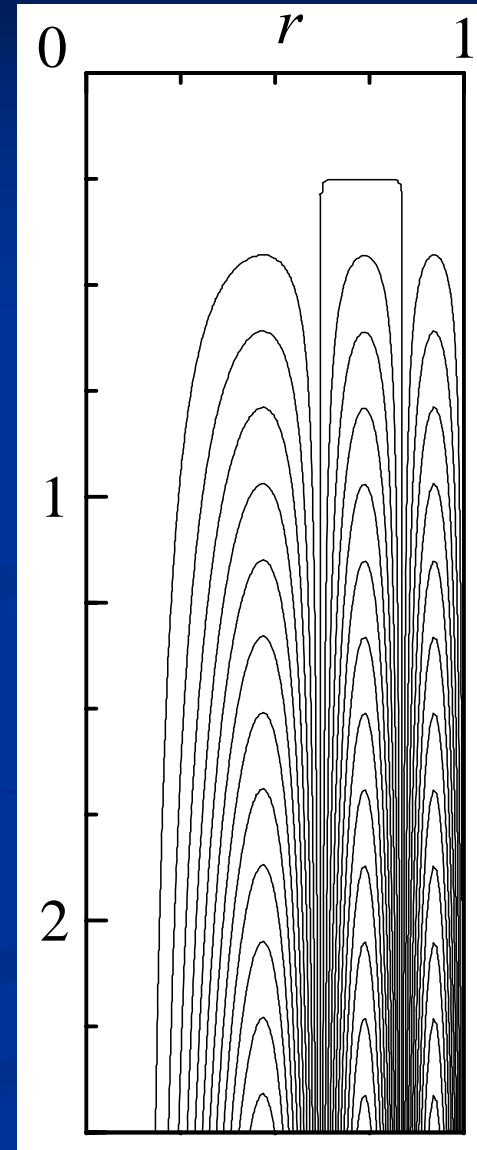
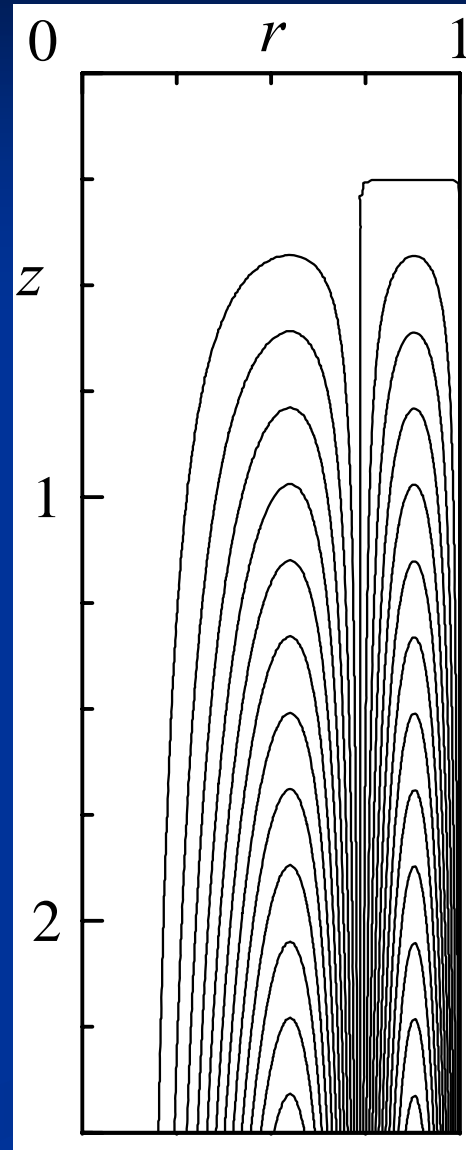
Temperature (K)



## Mantle Location (Under Reactive Flow Conditions)



# Multiple Solutions/Multi-Directional Flows (AIAA 2003-5054)





## Matrix of Mantle Locations

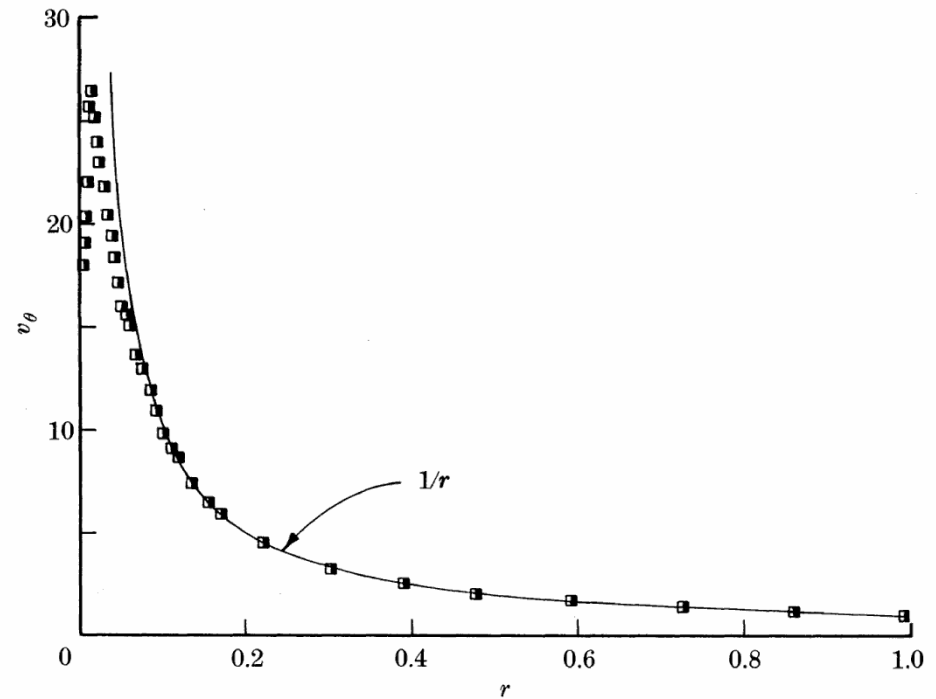
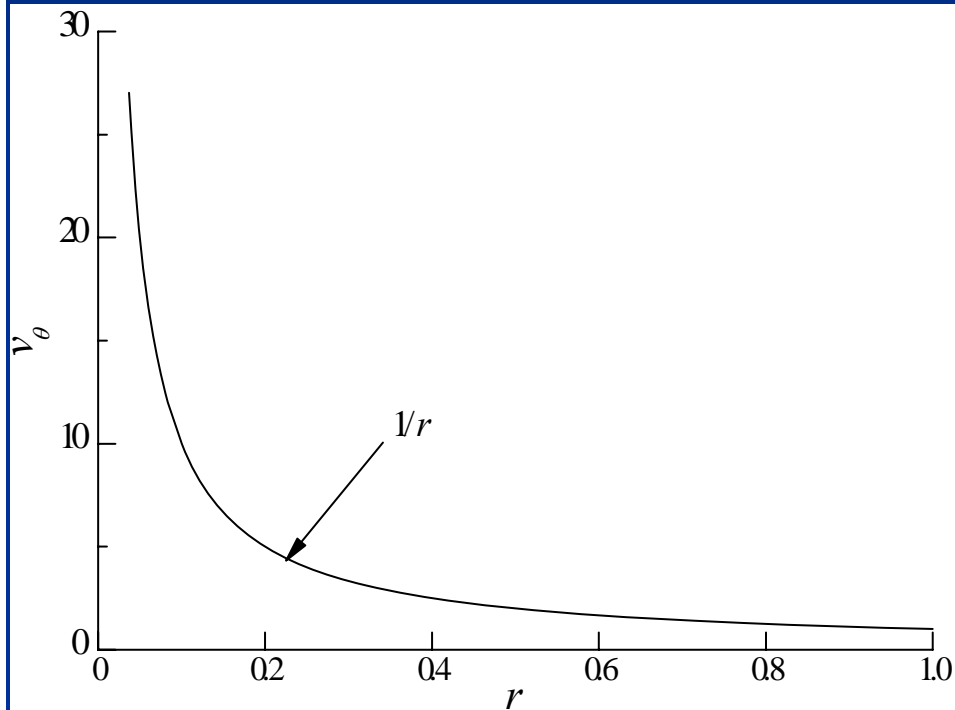
$$\beta_{m,n} = \sqrt{(n - \frac{1}{2}) / m}, \quad n = 1, 2, 3, \dots, m$$

$m$	$n = 1$	$n = 2$	$n = 3$	$n = 4$
1	$\beta_{1,1} = 1/\sqrt{2}$			
2	$\beta_{2,1} = 1/2$	$\beta_{2,2} = \sqrt{3}/2$		
3	$\beta_{3,1} = 1/\sqrt{6}$	$\beta_{3,2} = 1/\sqrt{2}$	$\beta_{3,3} = \sqrt{5/6}$	
4	$\beta_{4,1} = \sqrt{2}/4$	$\beta_{4,2} = \sqrt{6}/4$	$\beta_{4,3} = \sqrt{10}/4$	$\beta_{4,4} = \sqrt{14}/4$

Experimental Verification (Anderson AIAA 2003-4474)

Experimental image mantle locations (r/a)		Theoretical 4 mode mantle locations (r/a)		FLUENT Mantle locations (r/a)		Flow direction
0.594	0.803	0.612	0.791	0.385	0.787	down
0.803	0.955	0.791	0.935	0.787	1.00	up

## Singularity at the Center-Axis (AIAA 2003-5052)



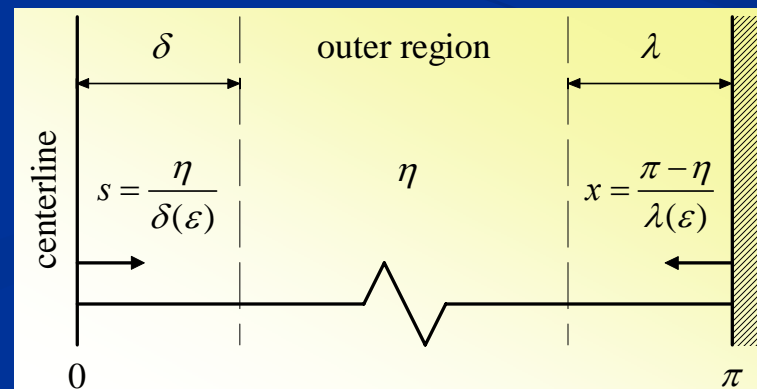
Phillips & Khoo (1987)  
Proc. Royal Soc., Vol. 411

# Viscous Tangential Momentum Equation (AIAA 2006-4888)

$$u_r \frac{\partial u_\theta}{\partial r} + \frac{u_r u_\theta}{r} = \frac{1}{Re} \left( \nabla^2 u_\theta - \frac{u_\theta}{r^2} \right); \quad Re \equiv \frac{Ua}{\nu}$$

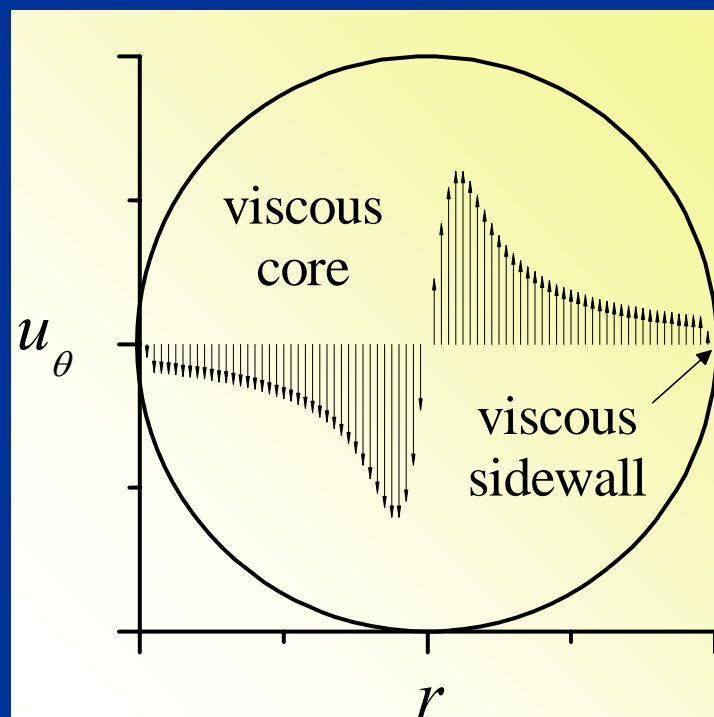
$$u_r \frac{du_\theta}{dr} + \frac{u_r u_\theta}{r} = \varepsilon \frac{d}{dr} \left[ \frac{1}{r} \frac{d(ru_\theta)}{dr} \right]; \quad \varepsilon \equiv \frac{1}{Re}$$

$$\begin{cases} r = 0, \quad \forall z, \quad u_\theta = 0 \\ r = 1, \quad z = l, \quad u_\theta = 1 \end{cases}$$

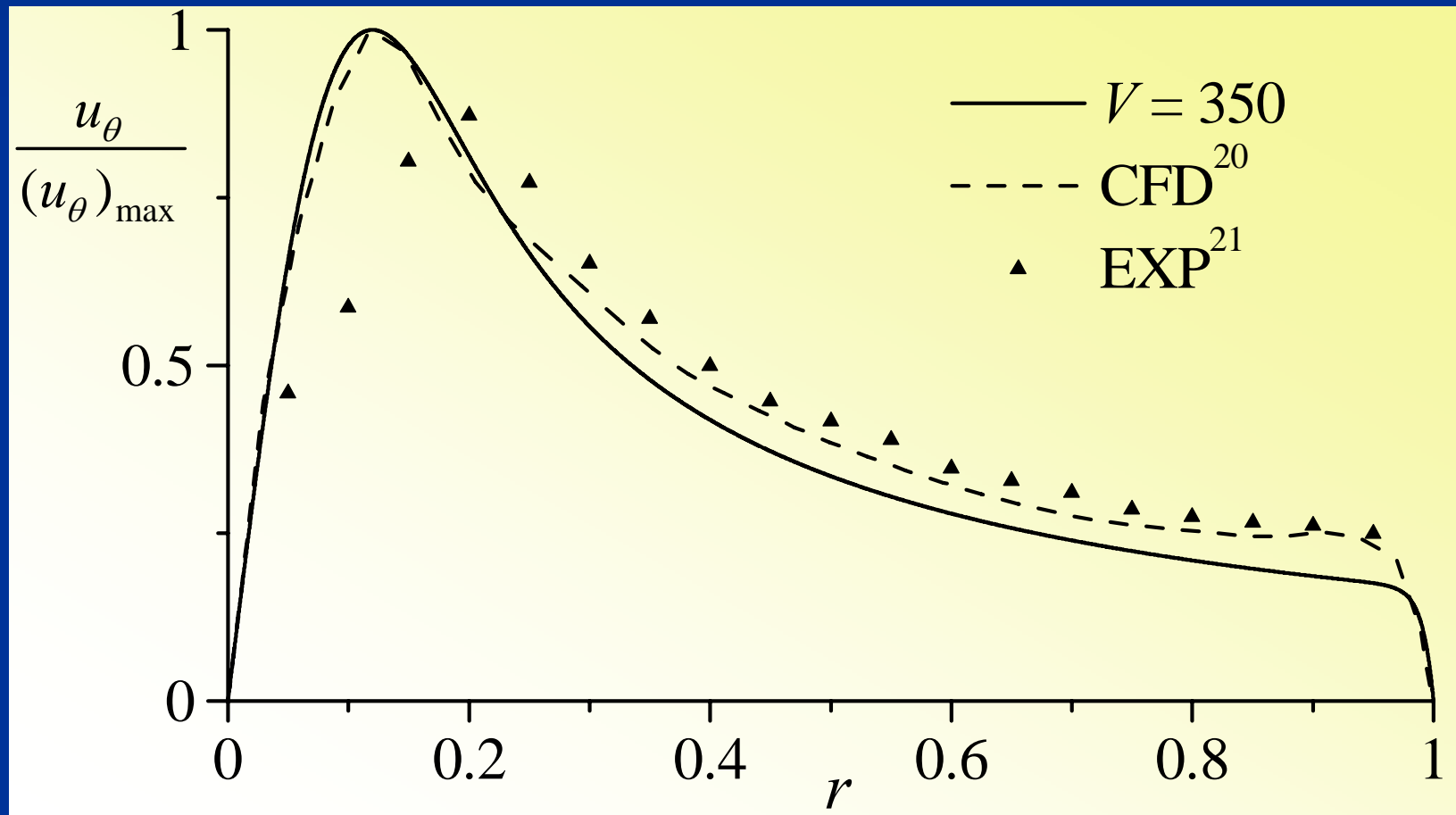


## Net Solution (AIAA 2006-4888)

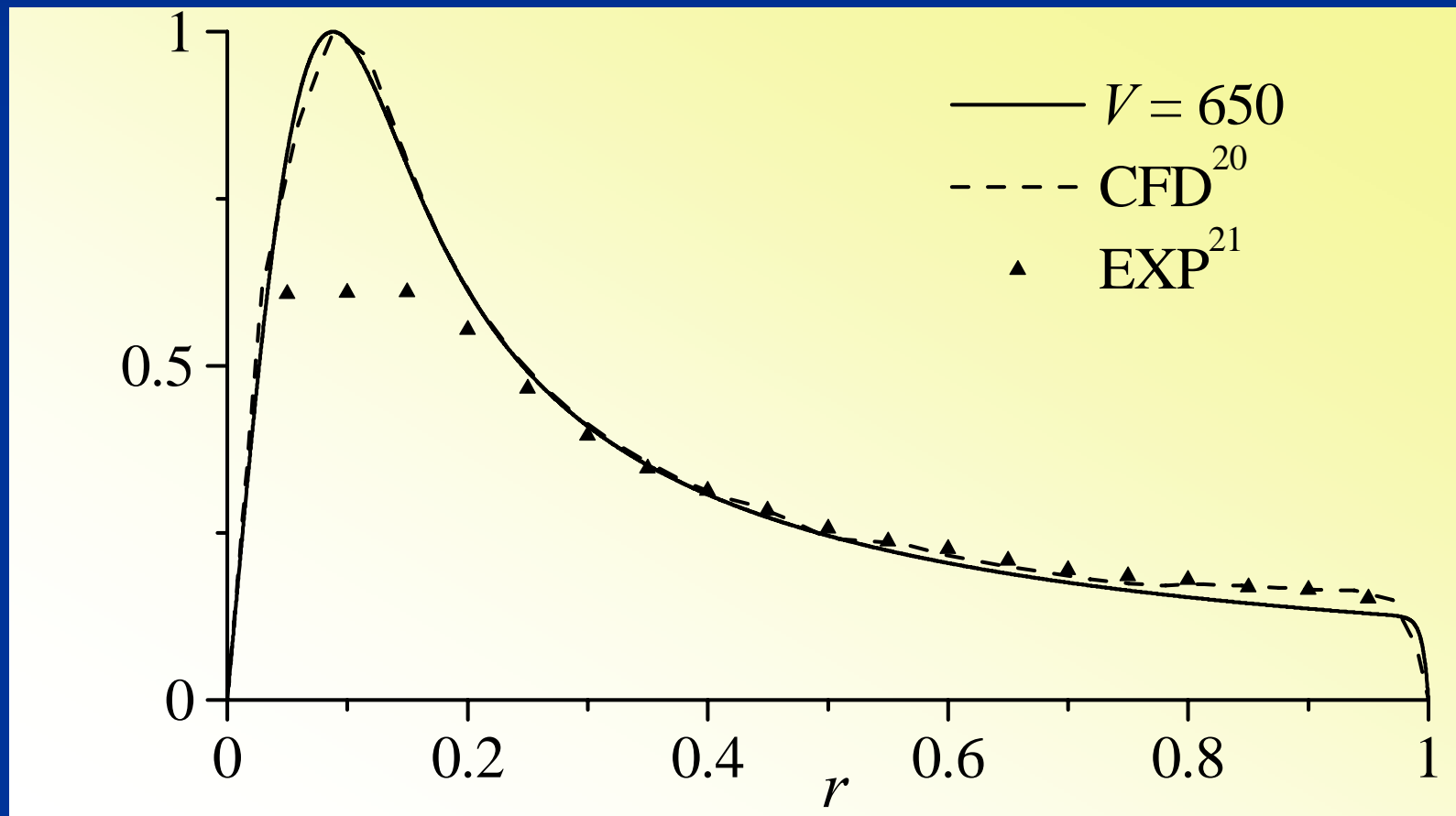
$$u_{\theta} = \begin{cases} \frac{1}{r} \left[ \frac{1 - e^{-\frac{1}{4}Vr^2}}{1 - e^{-\frac{1}{4}V}} + \frac{1 - e^{-\frac{1}{4}(\frac{1}{6}\pi^2 - 1)V(1-r^2)}}{1 - e^{-\frac{1}{4}(\frac{1}{6}\pi^2 - 1)V}} - 1 \right] \square \frac{1}{r} \left[ 1 - e^{-\frac{1}{4}Vr^2} - e^{-\frac{1}{4}(\frac{1}{6}\pi^2 - 1)V(1-r^2)} \right]; & 0 < z < l \\ \frac{1}{r} \left( \frac{1 - e^{-\frac{1}{4}Vr^2}}{1 - e^{-\frac{1}{4}V}} \right) \square \frac{1}{r} \left( 1 - e^{-\frac{1}{4}Vr^2} \right); & z = l \quad (\text{tangential injection at entry}) \end{cases}$$



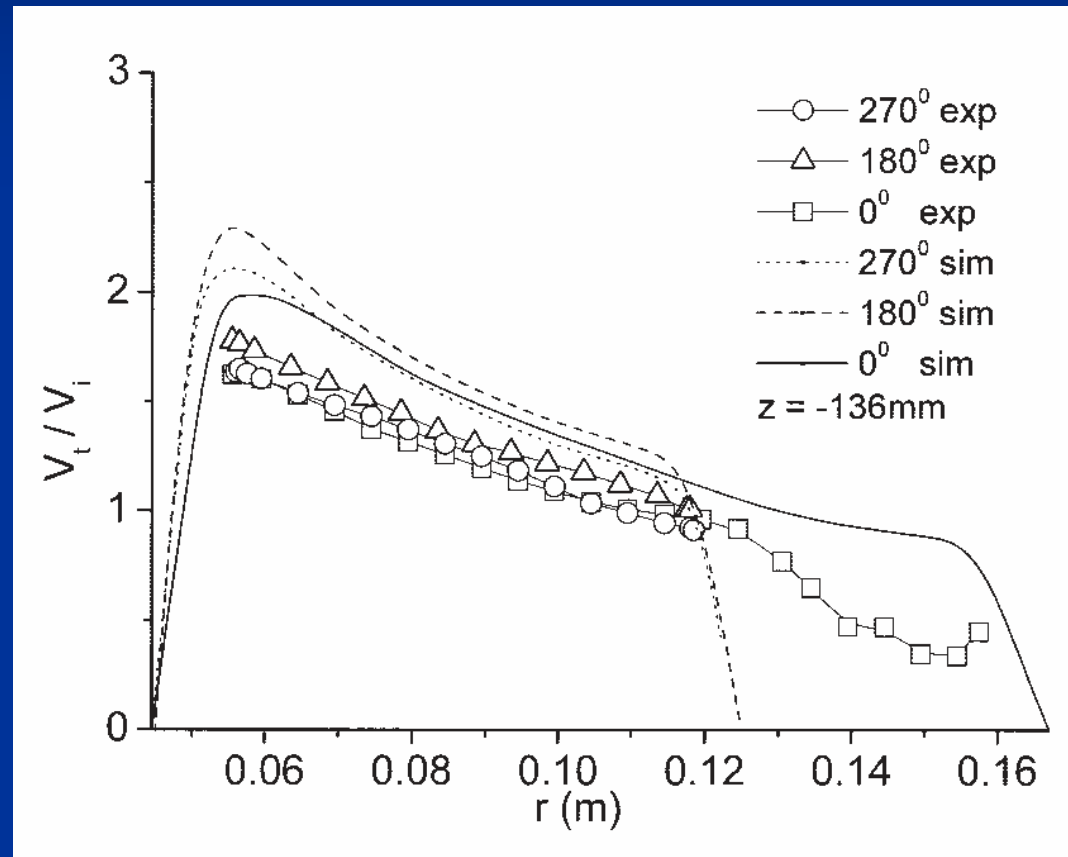
Comparison with Exp. and CFD::  
Rom, Anderson & Chiaverini, 2004-3359 (Exp)  
Murray *et al.*, 2004 (KIVA)



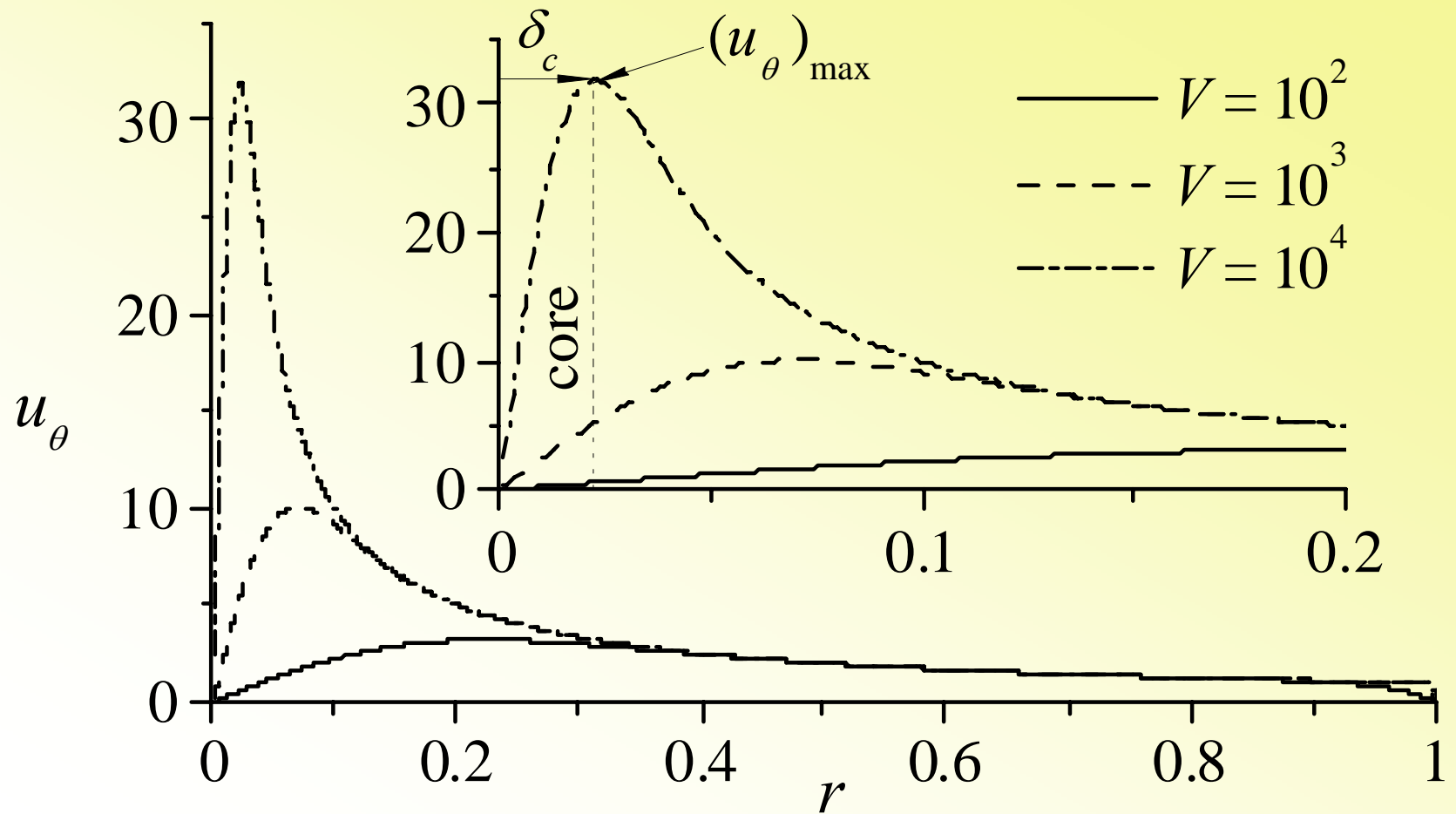
Comparison with Exp. and CFD::  
Rom, Anderson & Chiaverini, 2004-3359 (Exp)  
Murray *et al.*, 2004 (KIVA)



Other Experimental and CFD::  
Hu *et al.*, AICHE, Vol. 51, 2005

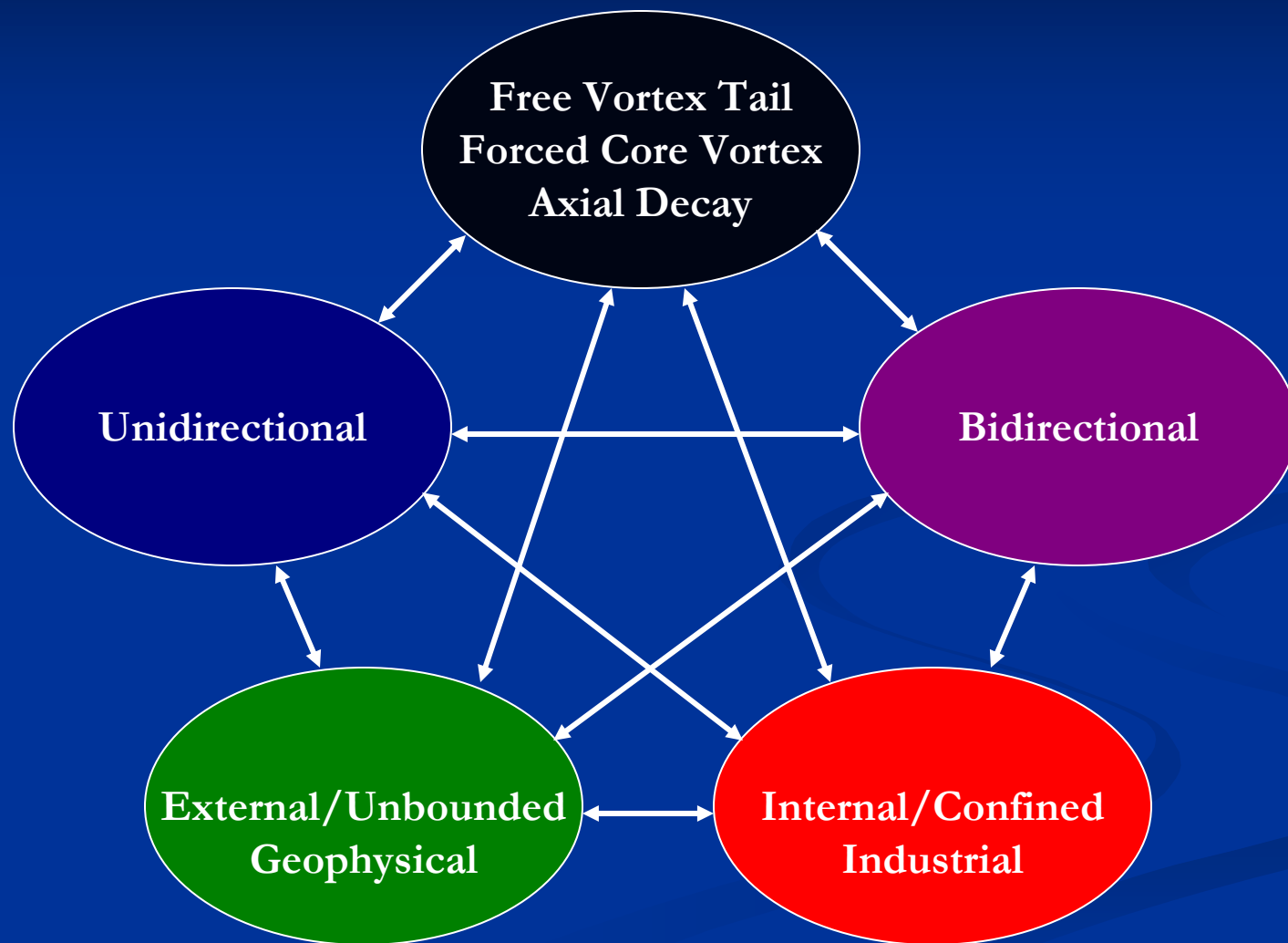


## Corrected Swirl Velocity





## Classification of Vortex/Swirl Dominated Flows



## Featured Results (AIAA 2006-4888)

$$V = \frac{1}{\varepsilon \sigma l} = \frac{a}{L} \frac{Re}{\sigma} = \frac{\rho \bar{Q}_i}{L \mu} = \text{vortex Reynolds no.}$$

$$\delta_c = \sqrt{-2 \left[ 1 + 2 \operatorname{pln} \left( p-1, -\frac{1}{2} e^{-\frac{1}{2}} \right) \right] / V} \approx 2.24 / V^{\frac{1}{2}}$$

$$\delta_w = 1 - \sqrt{1 + \frac{4 \ln \left\{ 0.01 + 0.99 \exp \left[ -\frac{1}{4} \left( \frac{1}{6} \pi^2 - 1 \right) V \right] \right\}}{\left( \frac{1}{6} \pi^2 - 1 \right) V}} \approx 1 - \sqrt{1 - \frac{4 \ln(100)}{\left( \frac{1}{6} \pi^2 - 1 \right) V}}$$

$$(u_\theta)_{\max} = \frac{1 - \exp \left[ \frac{1}{2} + \operatorname{pln} \left( p-1, -\frac{1}{2} e^{-\frac{1}{2}} \right) \right] \sqrt{V}}{\left( 1 - e^{-\frac{1}{4} V} \right) \sqrt{-2 \left[ 1 + 2 \operatorname{pln} \left( p-1, -\frac{1}{2} e^{-\frac{1}{2}} \right) \right]}} \approx 0.319 V^{\frac{1}{2}} \quad \boxed{\text{vortex strength}}$$

$$\omega = \frac{V}{4} \quad u_\theta = \omega r$$

## Other Key Findings

$$\tilde{Q} = \frac{2\pi \int_0^a \rho u_z u_\theta r dr}{\rho(\pi a^2) u_m^2} = \frac{\pi^2}{\sqrt{2}} \frac{C(1)\sigma}{(z/l)} = \frac{5.443}{(z/l)} \sigma$$

$$\sigma = \frac{\sqrt{2}}{\pi} S \approx 0.45S = \frac{1}{Q_i} = \frac{a^2}{A_i} \longleftrightarrow S = \frac{\pi}{4} \frac{d_e D}{A_i}$$

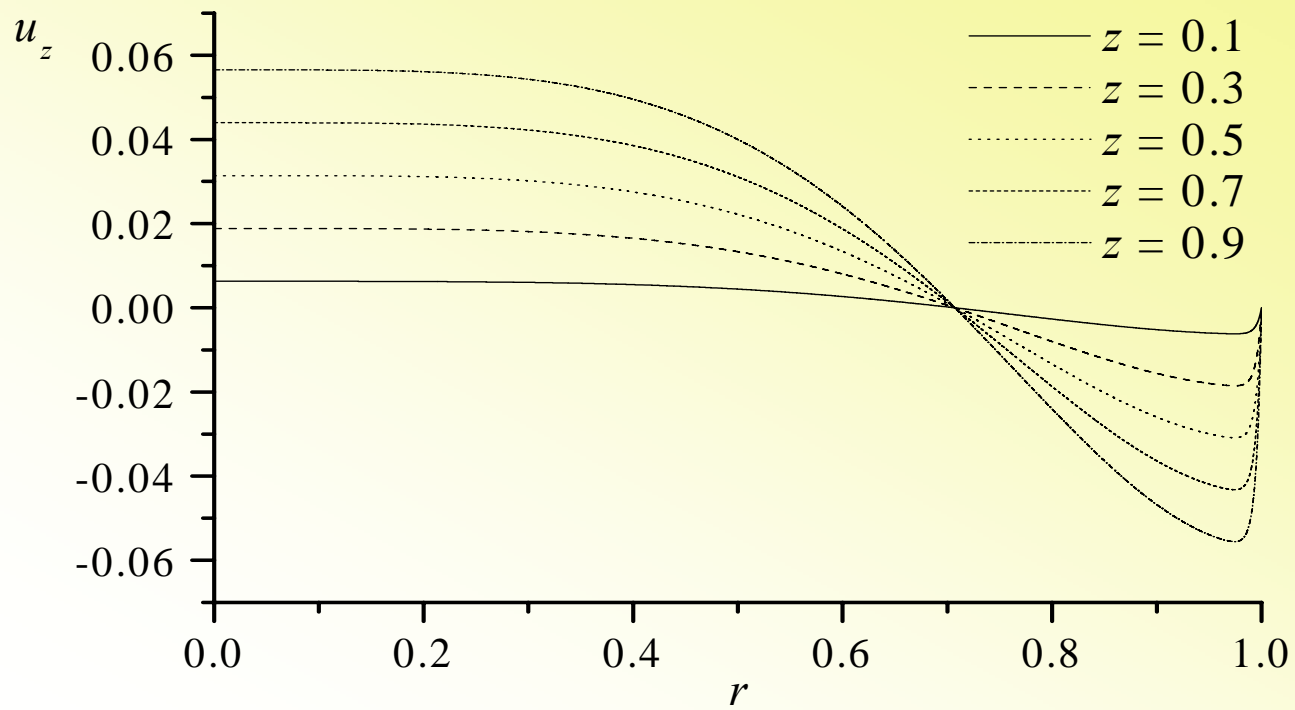
$$S_b = \sigma l = \frac{a^2 l}{A_i} = \frac{aL}{A_i}$$

## Sidewall Boundary Layer Corrections in the Axial Direction

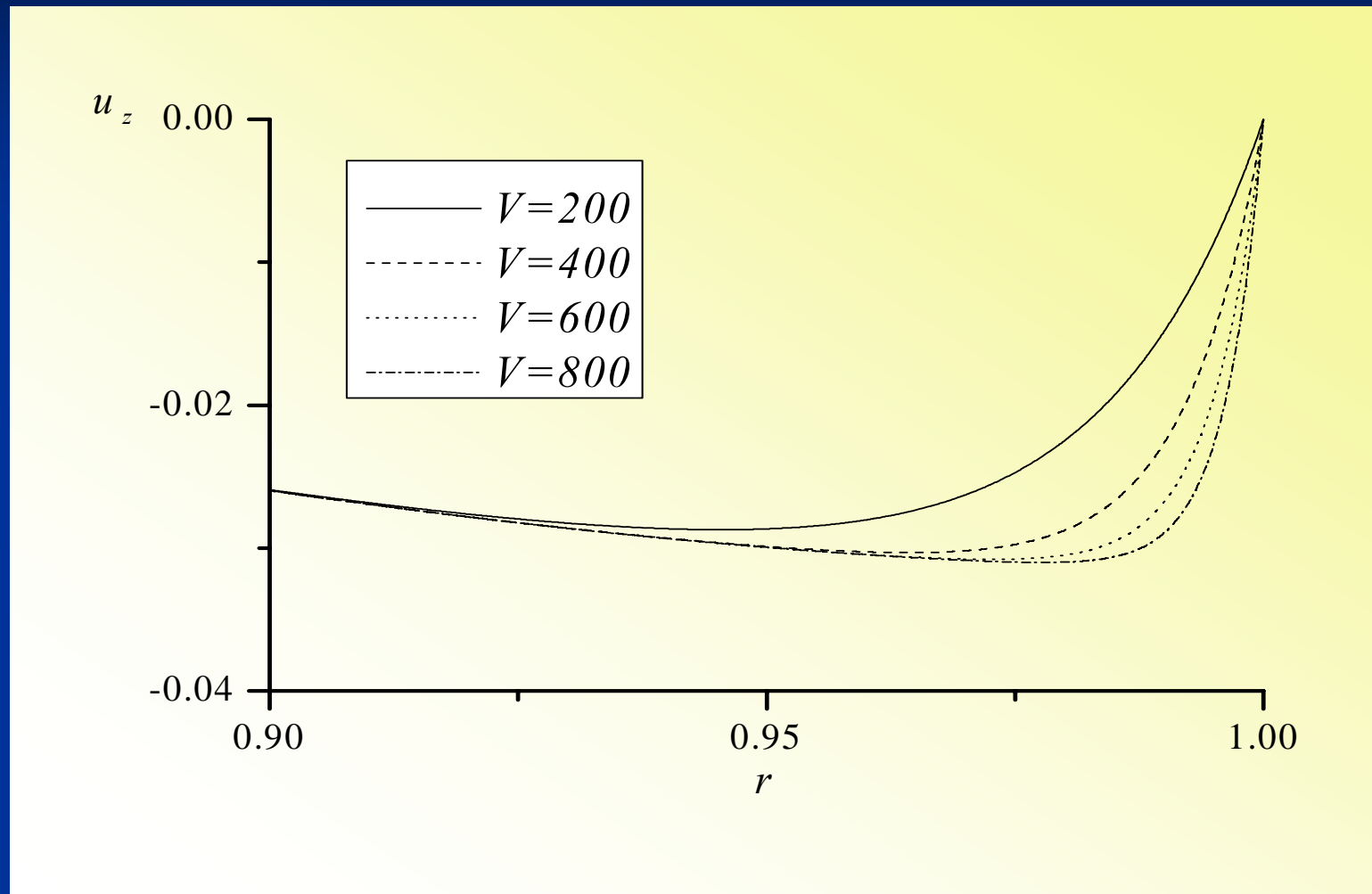
$$u_r \frac{\partial u_z}{\partial r} + u_z \frac{\partial u_z}{\partial z} = -\frac{\partial p}{\partial z} + \varepsilon \left( \frac{\partial^2 u_z}{\partial r^2} + \frac{1}{r} \frac{\partial u_z}{\partial r} \right); \quad \begin{cases} u_z(1, z) = 0 \\ \lim_{r \rightarrow 0} u_z(r, z) = U^o \end{cases}$$

$$u_z = 2\pi\kappa z \cos(\pi r^2) \left[ 1 - e^{-\frac{1}{4}V\left(\frac{1}{6}\pi^2 - 1\right)(1-r^2)} \right]$$

## Corrected Axial Velocity Profile



## Dependence on the Vortex Reynolds Number

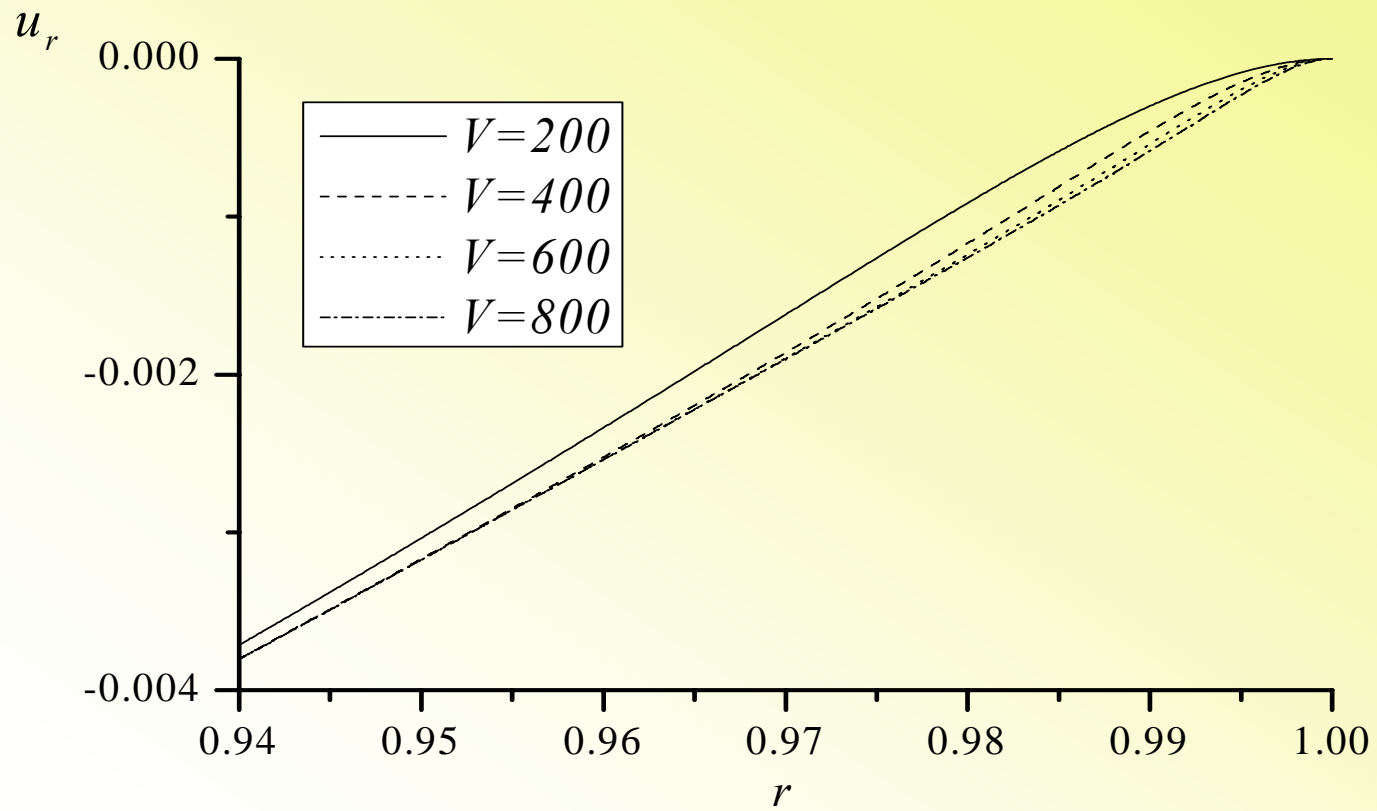


## Radial Corrections

$$\varepsilon \left( \frac{\partial^2 u_r}{\partial r^2} + \frac{1}{r} \frac{\partial u_r}{\partial r} - \frac{u_r}{r^2} \right) - u_r \frac{\partial u_r}{\partial r} + \frac{u_\theta^2}{r} - u_z \frac{\partial u_r}{\partial z} = \frac{\partial p}{\partial r}; \quad \begin{cases} u_r(1, z) = 0 \\ \lim_{r \rightarrow 0} u_r(r, z) = U^o \end{cases}$$

$$u_r(r, z) = -\frac{K}{r} \sin(\pi r^2) \left[ 1 - e^{-\frac{1}{4}V(\frac{1}{6}\pi^2 - 1)(1-r^2)} \right]$$

## Near Wall Radial Profile





## Comparison to Culick's Profile

Swirl-driven flow: Liquid vortex engine	Injection-driven flow: Solid rocket motor
$\mathbf{u} = u_r \mathbf{e}_r + u_\theta \mathbf{e}_\theta + u_z \mathbf{e}_z$ $u_r = -\frac{\kappa}{r} \sin(\pi r^2) \left[ 1 - e^{-\frac{V}{4}(\frac{\pi^2}{6}-1)(1-r^2)} \right]$ $u_\theta = \frac{1}{r} \left[ \frac{1 - e^{-\frac{V}{4}r^2}}{1 - e^{-\frac{V}{4}}} + \frac{1 - e^{-\frac{V}{4}(\frac{\pi^2}{6}-1)(1-r^2)}}{1 - e^{-\frac{V}{4}(\frac{\pi^2}{6}-1)}} - 1 \right]$ $u_z = 2\pi\kappa z \cos(\pi r^2) \left[ 1 - e^{-\frac{V}{4}(\frac{\pi^2}{6}-1)(1-r^2)} \right]$ $\boldsymbol{\Omega} = 4\pi^2\kappa r z \sin(\pi r^2) \mathbf{e}_\theta + \frac{V}{2} \left[ \frac{e^{-\frac{V}{4}r^2}}{1 - e^{-\frac{V}{4}}} - \frac{(\frac{\pi^2}{6}-1)e^{-\frac{V}{4}(\frac{\pi^2}{6}-1)(1-r^2)}}{1 - e^{-\frac{V}{4}(\frac{\pi^2}{6}-1)}} \right] \mathbf{e}_z$ $\psi = \kappa z \sin(\pi r^2)$	$\mathbf{u} = u_r \mathbf{e}_r + u_z \mathbf{e}_z$ $u_r = -\sin(\frac{1}{2} \pi r^2) / r$ $u_\theta = 0$ $u_z = \pi z \cos(\frac{1}{2} \pi r^2)$ $\boldsymbol{\Omega} = \pi^2 r z \sin(\frac{1}{2} \pi r^2) \mathbf{e}_\theta$ $\psi = z \sin(\frac{1}{2} \pi r^2)$
$\kappa \equiv \frac{1}{2\pi\sigma l} = \frac{A_i}{2\pi a L} \quad V \equiv \frac{Re}{\sigma} \frac{a}{L} = \frac{\bar{Q}_i}{Lv}$	Parameter free

## Motivations for Compressible Studies

- Greater understanding of the flow characteristics
- Verification of computational codes
- Approximate solutions useful for faster convergence in computational models
- Accurate foundation for modeling of flow field stability and thermal analysis

## Compressible Tangential Velocity

- Work in progress
- Three solution methods currently being investigated
  - Assuming the compressibility effects in the other directions are so small as to be negligible
  - Further reduce the compressible stream function, carrying only the most dominant terms for an approximate solution
  - Solve the compressible tangential momentum equation with the full stream function expression
- With the tangential velocity determined, the compressible bidirectional vortex will be fully defined

## Inviscid Compressible Formulation

$$D^2\psi^{(1)} + r\Omega^{(1)} = \nabla\rho^{(1)} \cdot \nabla\psi^{(0)} - r\Omega^{(0)}\rho^{(1)}$$

$$-\frac{1}{\gamma} \frac{\partial p^{(2)}}{\partial r} = \rho^{(1)} \left( u_0 \frac{\partial u_r^{(0)}}{\partial r} + u_z^{(0)} \frac{\partial u_r^{(0)}}{\partial z} - \frac{(u_\theta^{(0)})^2}{r} \right) + \frac{\partial(u_r^{(0)}u_r^{(1)})}{\partial r} + u_z^{(0)} \frac{\partial u_r^{(1)}}{\partial z} + u_z^{(1)} \frac{\partial u_r^{(0)}}{\partial z} - 2 \frac{u_\theta^{(0)}u_\theta^{(1)}}{r}$$

$$-\frac{1}{\gamma} \frac{\partial p^{(2)}}{\partial z} = \rho^{(1)} \left( u_z^{(0)} \frac{\partial u_z^{(0)}}{\partial z} + u_r^{(0)} \frac{\partial u_z^{(0)}}{\partial r} \right) + \frac{\partial(u_z^{(0)}u_z^{(1)})}{\partial z} + u_r^{(0)} \frac{\partial u_z^{(1)}}{\partial r} + u_r^{(1)} \frac{\partial u_z^{(0)}}{\partial r}$$

$$\rho^{(2)} = \frac{p^{(2)}}{\gamma} + \frac{1-\gamma}{2\gamma^2} (p^{(1)})^2$$

$$T^{(2)} = \frac{\gamma-1}{\gamma} p^{(2)} + \frac{1-\gamma}{2\gamma^2} (p^{(1)})^2$$

$$u_r^{(0)} \left( \frac{\partial u_\theta^{(1)}}{\partial r} + \frac{u_\theta^{(1)}}{r} \right) + u_r^{(1)} \left( \frac{\partial u_\theta^{(0)}}{\partial r} + \frac{u_\theta^{(0)}}{r} \right) = 0$$

## Singularity with the Inviscid, Compressible Formulation

$$u_r^{(1)}(0, z) = \frac{\rho^{(1)}}{r} \frac{\partial \psi^{(0)}}{\partial z} - \frac{1}{r} \frac{\partial \psi^{(1)}}{\partial z} = 0$$

$$u_r^{(0)} \left( \frac{\partial u_\theta^{(1)}}{\partial r} + \frac{u_\theta^{(1)}}{r} \right) + u_r^{(1)} \left( \frac{\partial u_\theta^{(0)}}{\partial r} + \frac{u_\theta^{(0)}}{r} \right) = 0$$

## Compressible Viscous Core Corrections

$$\varepsilon \frac{d^2 \xi^{(0)}}{d\eta^2} - \frac{u_r^{(0)}}{2\sqrt{\pi\eta}} \frac{d\xi^{(0)}}{d\eta} = 0 \quad (\text{leading-order eqn.})$$

$$\varepsilon \frac{d^2 \xi^{(1)}}{d\eta^2} - \frac{u_r^{(0)}}{2\sqrt{\pi\eta}} \frac{d\xi^{(1)}}{d\eta} - \frac{u_r^{(1)}}{2\sqrt{\pi\eta}} \frac{d\xi^{(0)}}{d\eta} - \frac{\rho^{(1)} u_r^{(0)}}{2\sqrt{\pi\eta}} \frac{d\xi^{(0)}}{d\eta} = 0 \quad (\text{first-order eqn.})$$

## Compressible Stream Function Correction

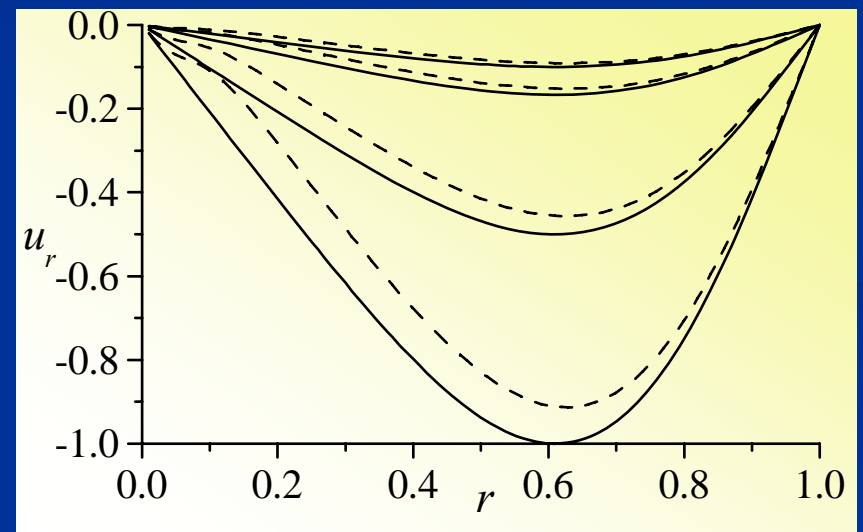
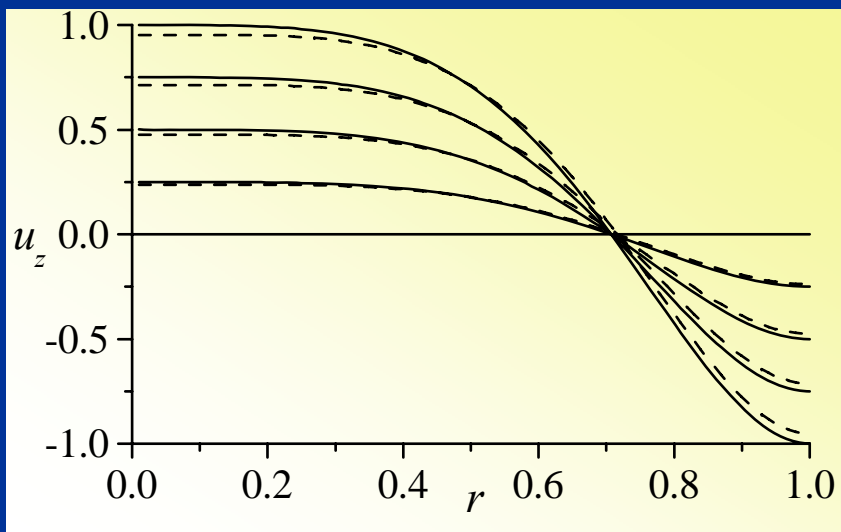
$$\begin{aligned} \psi^{(1)} = & \frac{\pi^2 B^3 z^3}{3} \sin(\pi r^2) \left[ 6 + \cos(2\pi r^2) - \cos(2\pi \beta^2) \right] + \frac{Bz}{8} e^{-r^2 V/2} \left[ (2e^{r^2 V/4} - 1) 4\pi \cos \pi r^2 \right. \\ & + e^{r^2 V/2} \left( \pi \cos \pi r^2 \left[ -2(2 + r^2 V) \text{Ei}\left(-\frac{r^2 V}{2}\right) + 2(4 + r^2 V) \text{Ei}\left(-\frac{r^2 V}{4}\right) - 2(4 + 9B^2) \ln r + (r^2 - 1)\phi \right] \right. \\ & \left. \left. + (\chi - \lambda) \sin \pi r^2 \right) \right] \end{aligned}$$

$$\phi = 4 + 4E - 12 \ln 2 + B^2 \ln 1024 \pi^9 + 4 \ln V$$

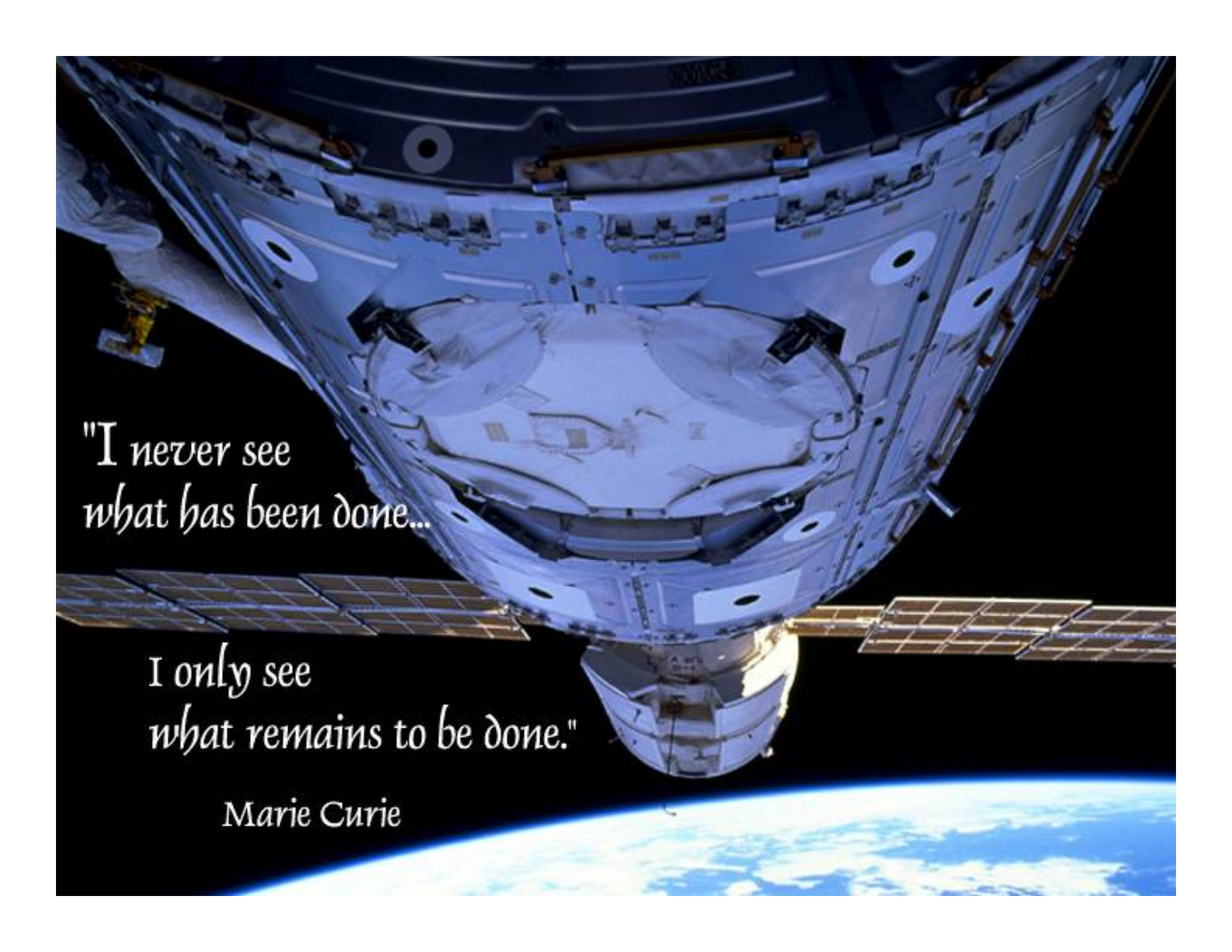
$$\chi = 2V \left( \tan^{-1} \frac{2\pi}{V} - \tan^{-1} \frac{4\pi}{V} \right) \csc \pi \beta^2$$

$$\lambda = \pi \csc \pi \beta^2 \left\{ \begin{aligned} & 4\text{Ci}(\pi \beta^2) + \ln \frac{1}{4096 \pi^4} + \cos \pi \beta^2 \left[ \ln 4096 + 4(\beta^2 - 1) \ln V \right] \\ & - 2 \ln(V^2 + 4\pi^2) + 4 \ln(V^2 + 16\pi^2) + 9B^2 \sin \pi \beta^2 \text{Si}(2\pi \beta^2) \end{aligned} \right\}$$

## Compressible vs Incompressible Velocity Results







*"I never see  
what has been done..."*

*I only see  
what remains to be done."*

Marie Curie

## Future Investigations (Part 1)

- Biglobal instability study
- Minimum Swirl no.
- Compressible BV (in progress)
- Compressible reactive model using the thin sheet approx.
- Endwall and sidewall boundary layers (in progress)
- Nusselt number correlation
- Mean flow interactions with particles

## Future Investigations (Part 2)

- BV in conical/spherical geometry (in progress)
- Perpetual self-reversing BV (fluid flywheel)
- Multi-directional solutions
- Breakdown patterns (S-shape, B-shape, etc)
- Dynamic evolution of wall temperatures by CFD
- Engine performance characteristics (thrust,  $I_{sp}$ ) using CFD (in progress)
- Resistance of the BV to acoustic oscillations
- Effect of roll torques on nozzle and flight motion